

Massive three-loop form factors: anomaly contribution

Matteo Fael^a, Fabian Lange^{b,c}, Kay Schönwald^d, Matthias Steinhauser^b

(a) *Theoretical Physics Department, CERN,*

1211 Geneva, Switzerland

(b) *Institut für Theoretische Teilchenphysik, Karlsruhe Institute of Technology (KIT),*

76128 Karlsruhe, Germany

(c) *Institut für Astroteilchenphysik, Karlsruhe Institute of Technology (KIT),*

76344 Eggenstein-Leopoldshafen, Germany

(d) *Physik-Institut, Universität Zürich, Winterthurerstrasse 190,*

8057 Zürich, Switzerland

Abstract

We compute three-loop corrections to the singlet form factors for massive quarks using a semi-analytic method which provides precise results over the whole kinematic range. Particular emphasis is put on the anomaly contribution originating from an external axial-vector current. We also discuss in detail the contribution for a pseudoscalar current and verify the chiral Ward identity to three-loop order. Explicit results are presented for the low- and high-energy regions and the expansions around threshold.

1 Introduction

Form factors are important building blocks in any quantum field theory. In QED and QCD they constitute the virtual corrections for many important processes both at lepton and hadron colliders such as Higgs boson production and decay, lepton pair production via the Drell-Yan process, and electron-muon scattering at low energies.

In this paper we consider QCD corrections to heavy-quark form factors of an external current. At one- and two-loop order such calculations have been performed already some time ago [1–11]. Recently we computed the three-loop corrections for the so-called non-singlet contributions, where the external current couples to the same fermion line as the external quarks [12, 13] (see also Refs. [8, 11, 14–17] for partial results of simpler subsets).¹ In Ref. [13] we also considered those singlet contributions where the external current couples to massive internal quarks, but only for vector, scalar, and pseudoscalar currents, i.e. omitting the axial-vector current. In this work we close this gap, compute all contributions for all four currents coupling to massless and massive quarks, and provide complete results for the singlet contributions. This requires a detailed discussion of the anomaly contribution for the axial-vector current following the line of the corresponding two-loop calculation of Ref. [5].

For completeness we want to mention that completely massless form factors are available up to four-loop order [19] (see Refs. [20–22] for the corresponding three-loop results). Three-loop corrections to massless form factors where the external current couples to massive quarks have been considered in Ref. [23]. This reference also contains a detailed discussion of the renormalization of the axial-vector current contribution. However, at three-loop order there are further subtleties for massive final-state quarks.

In the literature (see, e.g., Refs. [5, 24, 25]) one often finds the terms “flavour-singlet” and “flavour-non-singlet” which refer to certain combinations of (axial-vector) currents (and not to Feynman diagrams). The former is simply the sum of the axial-vector currents of the quarks involved in the theory. On the other hand, “flavour-non-singlet” refers to the difference of the axial-vector currents of the two quarks of a generation. The flavour-non-singlet current, which corresponds to the Z boson coupling in the SM, is conserved while the flavour-singlet current is anomalous.

In this paper we define “singlet” and “non-singlet” at the level of Feynman diagrams and use the notion:

- Singlet: The external current does not couple to the fermion line of the final-state quarks.
- Non-singlet: The external current couples directly to the fermion line of the final-state quarks.

¹Recently the total cross section for heavy-quark production at lepton colliders has been computed at next-to-next-to-next-to-leading order [18]. In this calculation the vector form factor enters as building block.

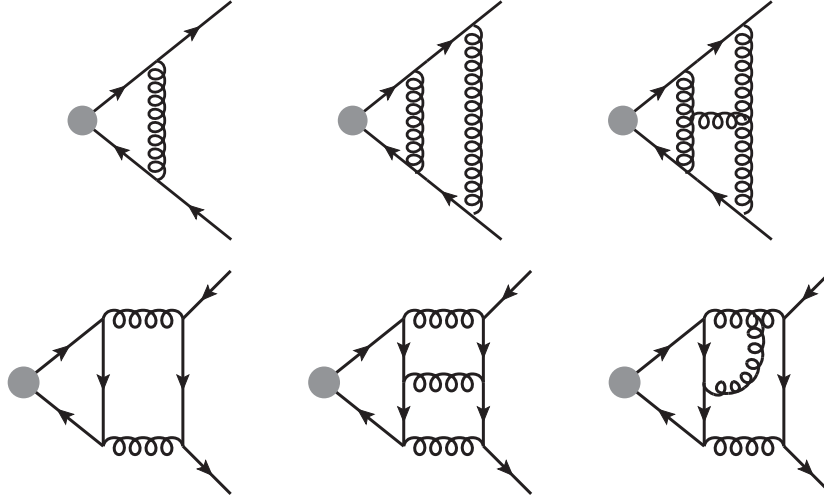


Figure 1: Sample Feynman diagrams contributing to the heavy-quark form factors. The top row displays non-singlet and the bottom row singlet diagrams up to three loops in QCD. The gray blob represents the coupling to the external current.

This is illustrated by the Feynman diagrams shown in Fig. 1, where the first and second row contain non-singlet and singlet contributions, respectively.

For the non-singlet contributions it is possible to use anti-commuting γ_5 . On the other hand, the singlet contributions require a definition of γ_5 in which traces of the form $\text{Tr}(\gamma_5 \gamma^\mu \gamma^\nu \gamma^\rho \gamma^\sigma)$ do not vanish. In this work we adopt the approach from Ref. [25], which is often called Larin scheme. Of course this prescription can also be applied to the non-singlet contributions. As a cross check we repeat the calculation of Ref. [13] and show that the final results for the finite form factors are identical in both prescriptions.

In the following we refer to massless and massive singlet contributions depending on whether the external current couples to massless or massive quarks, respectively. Results for the massive singlet form factors with external vector and scalar currents have already been presented in Ref. [13]. In this work we complete the massive and provide the massless singlet contributions.

For vector and scalar currents γ_5 is absent and thus these contributions can be treated in analogy to the non-singlet contributions. Since the vector current contribution vanishes at two-loop order due to Furry's theorem, it is finite at three-loop level. The scalar and pseudoscalar form factors only receive massive singlet contributions because the triangles vanish due to the Dirac algebra in the massless case. The results can be found in Ref. [13]. Note, however, that in Ref. [13] the finite renormalization constant for the pseudoscalar current has not been taken into account. In this work we correct this deficit. We consider the combination of the singlet and non-singlet contributions and introduce in both parts a non-anti-commuting γ_5 . As already mentioned above, the main focus of the present

work is on the axial-vector contribution.

The outline of this paper is as follows: In the next Section we introduce our notation and briefly mention our treatment of γ_5 . Afterwards we discuss the renormalization of the singlet form factors with special emphasis on the axial-vector current and the subtraction of infrared divergences. In Section 4 we discuss the chiral Ward identity and we dedicate Section 5 to the computation of the two- and three-loop vertex integrals and a discussion of the various cross checks which we have performed. Section 6 contains our results. Finally we conclude in Section 7. In Appendix A we explicitly state the projectors for the form factors and in Appendix B we provide all relevant renormalization constants related to the treatment of γ_5 . Appendix C contains explicit results for the massive singlet form factors and in Appendix D analytic results for the one- and two-loop expressions of the form factor induced by the pseudoscalar gluonic operator are presented. In Appendix E we provide a description of the package **FF31** where all results for the three-loop massive form factors are implemented.

2 Notation

We consider the vector (v), axial-vector (a), scalar (s), and pseudoscalar (p) currents

$$\begin{aligned}
j_\mu^v &= \bar{\psi}\gamma_\mu\psi, \\
j_\mu^a &= \bar{\psi}\gamma_\mu\gamma_5\psi, \\
j^s &= m\bar{\psi}\psi, \\
j^p &= im\bar{\psi}\gamma_5\psi.
\end{aligned}
\tag{1}$$

The factor m is introduced such that the scalar and pseudoscalar currents have vanishing anomalous dimensions.

It is convenient to decompose the three-point functions with an external quark-anti-quark pair into scalar form factors which we denote by

$$\begin{aligned}
\Gamma_\mu^v(q_1, q_2) &= F_1^v(q^2)\gamma_\mu - \frac{i}{2m}F_2^v(q^2)\sigma_{\mu\nu}q^\nu, \\
\Gamma_\mu^a(q_1, q_2) &= F_1^a(q^2)\gamma_\mu\gamma_5 - \frac{1}{2m}F_2^a(q^2)q_\mu\gamma_5, \\
\Gamma^s(q_1, q_2) &= mF^s(q^2), \\
\Gamma^p(q_1, q_2) &= imF^p(q^2)\gamma_5,
\end{aligned}
\tag{2}$$

where the momenta q_1 and q_2 are the momenta of the incoming quark and the outgoing anti-quark, respectively, which are on-shell, i.e. $q_1^2 = q_2^2 = m^2$. Furthermore, $q = q_1 - q_2$ is the outgoing momentum of the current with $q^2 = s$ and $\sigma_{\mu\nu} = i[\gamma_\mu, \gamma_\nu]/2$. The form factors F_i^k are conveniently obtained by applying appropriate projectors which we show in Appendix A. We denote the non-singlet and singlet contributions to the form factors

by²

$$F_{\text{non-sing}}^k \text{ and } F_{\text{sing},h/l}^k. \quad (3)$$

The second subscript h or l is used to distinguish the contributions where the external current couples to a massive or massless internal quark loop.

The colour structure of the two-loop singlet form factors is $C_F T_F$. For the three-loop singlet contributions we have altogether five colour structures: $C_F^2 T_F$, $C_F C_A T_F$, $C_F T_F^2 n_h$, $C_F T_F^2 n_l$ and $(d^{abc})^2/N_C$ where $C_F = T_F(N_C^2 - 1)/N_C$ and $C_A = 2T_F N_C$ are the quadratic Casimir operators of the $SU(N_C)$ gauge group in the fundamental and adjoint representation, respectively, n_l is the number of massless quark flavors, and $T_F = 1/2$. For convenience we introduce $n_h = 1$ for closed quark loops which have the same mass as the external quarks. We then denote the total number of quark flavors by $n_f = n_l + n_h$. Furthermore we have $(d^{abc})^2 = T_F^3(N_C^2 - 1)(N_C^2 - 4)/(2N_C)$. This colour structure only appears for the vector current, whereas the remaining four colour factors only appear for the axial-vector, scalar, and pseudoscalar currents.

For later convenience we introduce the perturbative expansion of the various (bare, renormalized, finite, ...) quantities as

$$F = \sum_{i \geq 0} \left(\frac{\alpha_s(\mu)}{\pi} \right)^i F^{(i)}, \quad (4)$$

where α_s depends on the number of active flavours. We perform the calculation of the bare diagrams and the renormalization of the ultraviolet counterterms in n_f -flavour QCD with $n_f = n_l + n_h$. We decouple the heavy quark from the running of α_s before subtracting the infrared poles (cf. Subsection 3.3) such that our final finite result for the form factors is parameterized in terms of $\alpha_s^{(n_l)}$. Note that in Eq. (4) the singlet diagrams start to contribute to $F^{(2)}$.

In case we implement the definition of γ_5 from Ref. [25] we replace it both in the Feynman rule for the current and in the projector for the axial-vector and pseudoscalar current according to

$$\begin{aligned} \gamma^\mu \gamma^5 &\rightarrow \frac{i}{3!} \varepsilon^{\mu\nu\rho\sigma} \gamma_{[\nu} \gamma_\rho \gamma_\sigma], \\ \gamma^5 &\rightarrow \frac{i}{4!} \varepsilon^{\mu\nu\rho\sigma} \gamma_{[\mu} \gamma_\nu \gamma_\rho \gamma_\sigma]. \end{aligned} \quad (5)$$

The square brackets on the r.h.s. denote anti-symmetrization of the corresponding indices. After applying the projectors we obtain products of two ε tensors which we replace by

$$\varepsilon_{\alpha_1 \alpha_2 \alpha_3 \alpha_4} \varepsilon_{\beta_1 \beta_2 \beta_3 \alpha_4} = |(\delta_{\alpha_i \beta_j})|. \quad (6)$$

The determinant on the r.h.s. of this equation is interpreted in $d = 4 - 2\epsilon$ dimensions.

²In Refs. [12,13] no subscript has been used for the non-singlet contribution.

3 Renormalization and infrared subtraction

In order to obtain the UV-renormalized form factors we perform a parameter renormalization for α_s in the $\overline{\text{MS}}$ and for the heavy-quark mass m in the on-shell scheme. In addition, we take into account the wave function renormalization for the external quarks in the on-shell scheme. For the scalar and pseudoscalar current we renormalize the factor m in the definition of the currents (see Eq. (1)) in the $\overline{\text{MS}}$ scheme.³

For the pseudoscalar and axial-vector currents there are additional renormalization constants which depend on the considered current and on the treatment of γ_5 . In the following we discuss in detail the renormalization of the corresponding form factors.

After renormalization the form factors still contain infrared poles. We discuss their subtraction in Subsection 3.3.

3.1 Pseudoscalar form factor F^p

The two-loop singlet diagram contributing to the pseudoscalar form factor does not develop sub-divergences and thus the form factor is finite. Similarly, at three-loop order the counterterm contributions from the quark wave function, α_s , m , and the overall renormalization constant related to the non-vanishing anomalous dimension of j^p are sufficient to render the three-loop singlet contributions ultraviolet finite. As a consequence it is not necessary to separate singlet and non-singlet contributions and we can consider the proper sum

$$F^{p,\text{bare}} = F_{\text{non-sing}}^{p,\text{bare}} + F_{\text{sing}}^{p,\text{bare}}, \quad (7)$$

and adopt the γ_5 prescription of Ref. [25] in all contributions. This leads to

$$F^p = Z_p^{\text{fin}} Z_p^{\overline{\text{MS}}} Z_2^{\text{OS}} F^{p,\text{bare}} \Bigg|_{m^{\text{bare}}=Z_m^{\text{OS}} m^{\text{OS}}, \alpha_s^{\text{bare}}=Z_{\alpha_s} \alpha_s}, \quad (8)$$

where Z_2^{OS} is the on-shell wave function renormalization constant for the external quarks.

In case we drop the singlet contributions and use anti-commuting γ_5 we have $Z_p^{\text{fin}} = 1$ and $Z_p^{\overline{\text{MS}}} = Z_m^{\overline{\text{MS}}}$ in the above formula, where $Z_m^{\overline{\text{MS}}}$ is the $\overline{\text{MS}}$ renormalization constant of the quark mass. For the γ_5 prescription of Ref. [25] explicit results for Z_p^{fin} and $Z_p^{\overline{\text{MS}}}$ can be found in Eq. (50). It is a welcome cross check of our calculation that the non-singlet contribution of F^p agrees in the two approaches up to three-loop order.

The results for F_{sing}^p have already been shown in Ref. [13]. However, in this reference $Z_p^{\text{fin}} = 1$ has been chosen and Z_m^{OS} has been used instead of $Z_p^{\overline{\text{MS}}}$. This has, of course, no influence on the finiteness of the form factor (after infrared subtraction), but the finite terms differ.

³Note that in Ref. [13] the factor m has been renormalized in the $\overline{\text{MS}}$ scheme for the non-singlet current. However, for the singlet currents the on-shell scheme has been used.

3.2 Axial-vector form factors F_1^a and F_2^a

The singlet diagram contributions to the axial-vector form factor develop the famous Adler-Bell-Jackiw anomaly [26, 27] which leads to a rather non-trivial renormalization. In our derivation we assume that all $n_f = n_l + n_h$ quarks are grouped into doublets and $n_h = 1$. We then introduce the “flavour-non-singlet” current

$$J_{\text{NS},\mu}^a = \sum_{i=1}^{n_f} a_i \bar{\psi}_i \gamma_\mu \gamma_5 \psi_i, \quad (9)$$

where a_i is the coupling of the quarks to the Z boson in the SM. For us it is sufficient to assume $a_i = \pm 1$ depending on the weak isospin of the quark. The sum in Eq. (9) is to be understood such that the massive form factors of quark flavour i originating from $J_{\text{NS},\mu}^a$ can be written as

$$F_{i,\text{NS}}^a = F_{i,\text{non-sing}}^a + F_{i,\text{sing},h}^a - F_{i,\text{sing},l}^a, \quad (10)$$

where $F_{i,\text{sing},h}^a$ and $F_{i,\text{sing},l}^a$ denote the massive and massless singlet contributions as introduced in Section 2, respectively. The relative sign between $F_{i,\text{sing},h}^a$ and $F_{i,\text{sing},l}^a$ guarantees the anomaly cancellation in the SM. It is well known that $J_{\text{NS},\mu}^a$ renormalizes multiplicatively which also holds for the form factors

$$F_{i,\text{NS}}^a = Z_{\text{NS}} Z_2^{\text{OS}} F_{i,\text{NS}}^{a,\text{bare}}, \quad (11)$$

where parameter renormalization on the r.h.s. in analogy to Eq. (8) is understood. The renormalization constant Z_{NS} can be decomposed into

$$Z_{\text{NS}} = Z_{a,\text{NS}}^{\text{fin}} Z_{a,\text{NS}}^{\overline{\text{MS}}} \quad (12)$$

with the $\overline{\text{MS}}$ renormalization constant $Z_{a,\text{NS}}^{\overline{\text{MS}}}$ and the finite renormalization $Z_{a,\text{NS}}^{\text{fin}}$. Up to the required order $Z_{a,\text{NS}}^{\text{fin}}$ and $Z_{a,\text{NS}}^{\overline{\text{MS}}}$ can be found in Eq. (49) in Appendix B.

We also define the “flavour-singlet” current

$$J_{\text{S},\mu}^a = \sum_{i=1}^{n_f} \bar{\psi}_i \gamma_\mu \gamma_5 \psi_i, \quad (13)$$

where all quarks couple to the axial-vector current with the same sign. Hence the form factors decompose into

$$F_{i,\text{S}}^a = F_{i,\text{non-sing}}^a + F_{i,\text{sing},h}^a + \sum_{j=1}^{n_l} F_{i,\text{sing},j}^a. \quad (14)$$

Again the current and the form factors renormalize multiplicatively, i.e.

$$F_{i,\text{S}}^a = Z_{\text{S}} Z_2^{\text{OS}} F_{i,\text{S}}^{a,\text{bare}}, \quad (15)$$

where

$$Z_S = Z_{a,S}^{\text{fin}} Z_{a,S}^{\overline{\text{MS}}} \quad (16)$$

can be decomposed in the same manner as Z_{NS} in Eq. (12). We again refer to Eq. (49) for the explicit renormalization constants.

With these definitions one can derive the renormalization for the non-singlet and singlet axial-vector form factors $F_{i,\text{sing}}^a$ and $F_{i,\text{non-sing}}^a$. In the non-singlet case we have a multiplicatively renormalization without any interference of the singlet diagram contributions. It is given by

$$F_{i,\text{non-sing}}^a = Z_{\text{NS}} Z_2^{\text{OS}} F_{i,\text{non-sing}}^{a,\text{bare}}. \quad (17)$$

On the other hand, for the renormalized singlet diagram contributions we have to consider the difference $\frac{1}{n_f}(F_{i,S}^a - F_{i,\text{NS}}^a)$. Since the SM is anomaly free, $F_{i,\text{sing},h}^{a,\text{bare}}$ and $F_{i,\text{sing},l}^{a,\text{bare}}$ have to renormalize in the same way and one finds (see also Ref. [23])

$$F_{i,\text{sing},j}^a = Z_{\text{NS}} Z_2^{\text{OS}} F_{i,\text{sing},j}^{a,\text{bare}} + \frac{1}{n_f} (Z_S - Z_{\text{NS}}) Z_2^{\text{OS}} \left(F_{i,\text{non-sing}}^{a,\text{bare}} + \sum_{k=1}^{n_f} F_{i,\text{sing},k}^{a,\text{bare}} \right), \quad (18)$$

where $j \in \{h, l\}$ and

$$\begin{aligned} \frac{1}{n_f} (Z_S - Z_{\text{NS}}) &= Z_{a,S}^{\text{fin}} Z_{a,S}^{\overline{\text{MS}}} - Z_{a,\text{NS}}^{\text{fin}} Z_{a,\text{NS}}^{\overline{\text{MS}}} \\ &= \left(\frac{\alpha_s}{\pi} \right)^2 C_F T_F \left(\frac{3}{8\epsilon} + \frac{3}{16} \right) + \left(\frac{\alpha_s}{\pi} \right)^3 C_F T_F \left(\frac{1}{\epsilon^2} \left[\frac{1}{12} T_F (n_h + n_l) \right. \right. \\ &\quad \left. \left. - \frac{11}{48} C_A \right] + \frac{1}{\epsilon} \left[\frac{109}{288} C_A - \frac{9}{16} C_F + \frac{1}{72} T_F (n_h + n_l) \right] + \left[\frac{13}{16} \zeta_3 - \frac{163}{864} \right] C_A \right. \\ &\quad \left. - \left[\frac{3}{4} \zeta_3 - \frac{23}{64} \right] C_F + \frac{11}{54} T_F (n_h + n_l) \right) + \mathcal{O}(\alpha_s^4). \end{aligned} \quad (19)$$

Again we implicitly assume parameter renormalization in analogy to Eq. (8).

Since $(Z_S - Z_{\text{NS}})$ starts at $\mathcal{O}(\alpha_s^2)$, we need $F_{i,\text{non-sing}}^{a,\text{bare}}$ only to one-loop order and the last term on the right-hand-side can be neglected. It is crucial to use the same prescription for γ_5 both in the calculation of $F_{i,\text{sing},j}^{a,\text{bare}}$ and $F_{i,\text{non-sing}}^{a,\text{bare}}$. Furthermore, it is important to keep the higher-order terms in ϵ in the tree-level expression $F_{i,\text{non-sing}}^{a,\text{bare},(0)}$. For example, the α_s^3/ϵ^2 term of $(Z_S - Z_{\text{NS}})$ multiplies the $\mathcal{O}(\epsilon)$ term of $F_{i,\text{non-sing}}^{a,\text{bare},(0)}$ and produces a term proportional to α_s^3/ϵ which is necessary to cancel all poles for the $C_A C_F T_F$ and $C_F T_F^2$ colour factors. The finiteness of the $C_F^2 T_F$ colour factor is guaranteed through the $\mathcal{O}(\alpha_s^2)$ term of $(Z_S - Z_{\text{NS}})$ which multiplies $F_{1,\text{non-sing}}^{a,(1),\text{bare}}$.

3.3 Infrared divergences

After the ultraviolet renormalization we still have infrared poles which we treat via

$$F^f = Z^{-1} F, \quad (20)$$

where F is the UV renormalized form factor and F^f is finite, i.e., the limit $\epsilon \rightarrow 0$ can be taken. Z can be constructed from the cusp anomalous dimension which has been computed to three-loop order in Refs. [28–31]. In our calculation we express F^f in terms of $\alpha_s^{(n_i)}$.

4 Chiral Ward identity

For the axial-vector current the non-renormalization of the Adler-Bell-Jackiw (ABJ) anomaly implies that the equation

$$(\partial^\mu j_\mu^a)_R = 2(j^p)_R + \frac{\alpha_s}{4\pi} T_F(G\tilde{G})_R \quad (21)$$

holds at the level of renormalized operators (indicated by the subscript R) [32]. It relates the derivative of the axial-vector current to the pseudoscalar current and the pseudoscalar gluonic operator

$$G\tilde{G} = \epsilon_{\mu\nu\rho\sigma} G^{a,\mu\nu} G^{a,\rho\sigma}, \quad (22)$$

where $G^{a,\mu\nu}$ is the field strength tensor of the gluon. In analogy to Eq. (2) the three-point functions of $\partial^\mu j_\mu^a$ and $G\tilde{G}$ with a massive quark-anti-quark pair can be decomposed as

$$\begin{aligned} \Gamma_{\partial J}^a(q_1, q_2) &= 2imF_{\partial J}(q^2)\gamma_5, \\ \Gamma_{G\tilde{G}}(q_1, q_2) &= 2imF_{G\tilde{G}}(q^2)\gamma_5, \end{aligned} \quad (23)$$

with the form factors $F_{\partial J}$ and $F_{G\tilde{G}}$. This allows us to rewrite Eq. (21) at the level of form factors as

$$F_{\partial J, \text{non-sing}} = F_{\text{non-sing}}^{p,f} \quad (24)$$

for the non-singlet and

$$F_{\partial J, \text{sing}} = F_{\text{sing}}^{p,f} + \frac{\alpha_s}{4\pi} T_F F_{G\tilde{G}}^f \quad (25)$$

for the singlet contributions. Equations (24) and (25) are usually referred to as chiral Ward identities, the latter especially as the anomalous chiral Ward identity. In this work we use them as non-trivial cross checks of our results. This is particularly interesting for Eq. (25) which involves finite renormalization constants related to the treatment of γ_5 .

For this check we require $F_{G\tilde{G}}^f$ to $\mathcal{O}(\alpha_s^2)$. Since the operators $G\tilde{G}$ and $\partial^\mu j_\mu^a$ mix under renormalization, the finite expression is given by

$$F_{G\tilde{G}}^f = Z^{-1} Z_2^{\text{OS}} (Z_{G\tilde{G}} F_{G\tilde{G}}^{\text{bare}} + Z_{GJ} F_{\partial J}^{\text{bare}}) \Big|_{m^{\text{bare}}=Z_m^{\text{OS}} m^{\text{OS}}, \alpha_s^{\text{bare}}=Z_{\alpha_s} \alpha_s}. \quad (26)$$

The renormalization constants $Z_{G\tilde{G}}$ and Z_{GJ} have been computed in Refs. [25, 33–37]. To the required orders they read

$$Z_{G\tilde{G}} = Z_{\alpha_s} = 1 + \frac{\alpha_s}{\pi} \frac{1}{\epsilon} \left(-\frac{11}{12} C_A + \frac{1}{3} T_F n_f \right) + \mathcal{O}(\alpha_s^2),$$

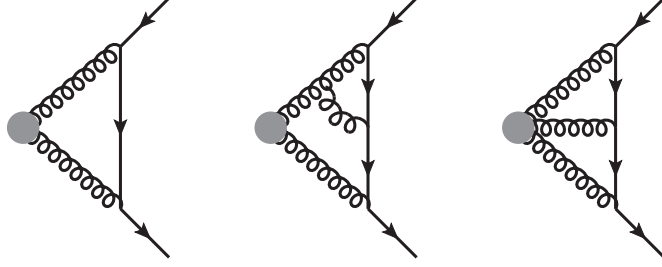


Figure 2: One- and two-loop sample Feynman diagrams contributing to $F_{G\tilde{G}}$.

$$\begin{aligned}
Z_{GJ} = & \frac{\alpha_s}{\pi} \frac{3C_F}{\epsilon} + \left(\frac{\alpha_s}{\pi}\right)^2 \left(\frac{1}{\epsilon^2} \left[C_F n_f T_F - \frac{11}{4} C_A C_F \right] + \frac{1}{\epsilon} \left[\frac{71}{24} C_A C_F \right. \right. \\
& \left. \left. - \frac{21}{8} C_F^2 - \frac{1}{6} C_F T_F n_f \right] \right) + \mathcal{O}(\alpha_s^3). \tag{27}
\end{aligned}$$

The factor Z^{-1} again subtracts infrared poles, cf. Subsection 3.3. We thus have to compute one- and two-loop corrections for $F_{G\tilde{G}}$ and one-loop corrections to $F_{\partial J}$ since Z_{GJ} starts at $\mathcal{O}(\alpha_s)$.

We compute $F_{G\tilde{G}}^{\text{bare}}$ using the same setup as for the other form factors which is described in Section 5. Sample Feynman diagrams contributing to it are shown in Fig. 2. We apply the same projector as for the pseudoscalar current and use the prescription of γ_5 from Eq. (5).

To compute $F_{\partial J}$ we follow two different strategies: First we treat $\partial^\mu j_\mu^a$ as an independent operator, implement its Feynman rule using Eq. (5), and then apply again the projector to the pseudoscalar current. Secondly we apply the derivative to Γ_μ^a in its decomposed form of Eq. (2) and employ the Dirac equation as well as an anti-commuting γ_5 to find

$$F_{\partial J} = F_1^{a,f} + \frac{S}{4m^2} F_2^{a,f}. \tag{28}$$

Thus we can simply use the expressions for $F_1^{a,f}$ and $F_2^{a,f}$ directly instead of computing $F_{\partial J}$. Both approaches lead to identical results. It is interesting to mention that the higher order ϵ terms of the tree-level expression

$$F_{\partial J}^{(0)} = 1 - \frac{11\epsilon}{3} + 4\epsilon^2 - \frac{4\epsilon^3}{3}, \tag{29}$$

are crucial to obtain the correct result, at least with our choice of projectors, cf. Appendix A.

After inserting the bare results and counterterms into Eq. (26) we obtain a finite result for $F_{G\tilde{G}}^f$ which we present in Appendix D. This then allows us to check the anomalous Ward identity (24) in Subsection 5.3.

5 Computational details

For our calculation we use the same automated setup as for the calculation of the non-singlet form factors in Refs. [12,13]. We generate the diagrams with `qgraf` [38] and process them with `q2e` and `exp` [39–41] to obtain `FORM` [42] code for each individual amplitude. After applying the projectors and taking the traces each amplitude is written as a linear combination of scalar functions which belong to certain integral families. The reduction to master integrals is performed with `Kira` [43,44] with `Fermat` [45]. At this step it is important to choose a good basis where the dependence on the kinematic variable and the space-time factorizes. For this step we use the program `ImproveMaster.m` developed in Ref. [46] in an improved version. Once we know the master integrals for each individual integral family we use `Kira` to find a minimal set which reduces the number of master integrals from 1995 to 316 for the massive and from 698 to 158 for massless singlet contributions. Next we establish the differential equations with the help of `LiteRed` [47,48]. At this point only the boundary conditions of all master integrals at some initial value for s/m^2 are needed such that the method of Ref. [49] can be applied to obtain results for all master integrals in the whole kinematic range. We already computed the master integrals for the massive singlet contributions in Ref. [13]. Thus we only describe the calculation of the massless singlet contributions in Subsection 5.1.

The calculation of $F_{G\bar{G}}$ follows the same general setup. However, instead of `q2e` we use `tapir` [50]. The different mass patterns require the introduction of new integral families which lead to 3 and 24 master integrals at one- and two-loop order, respectively. 9 of the two-loop master integrals are known from the two-loop calculation of the non-singlet form factors. We describe the analytical computation of the remaining 15 master integrals in Subsection 5.2.

5.1 Computation of massive vertex integrals at three loops

The method for our calculation of the three-loop master integrals is described in detail in Ref. [13]. We deviate slightly from the steps outlined in this reference by not computing analytical boundary conditions in the asymptotic limit $s \rightarrow 0$. Instead we use numerical boundary conditions obtained with `AMFlow` [51]⁴ at $s/m^2 = -1$ which corresponds to a regular point. More precisely, we use `AMFlow` with `Kira` [43,44] as reduction back-end to compute all master integrals as expansions up to ϵ^6 at $s/m^2 = -1$. The coefficients of these expansions are floating point numbers which we obtain with 100 significant digits within a few days of runtime for all integral families except one for which we obtain only 85 significant digits. From there we derive symbolic expansion at

$$s/m^2 = \{-\infty, -32, -28, -24, -16, -12, -8, -4, -3, -2, -1, -3/4, -1/2, -1/4, 0, 1/4, 1/2, 1, 2, 3, 7/2, 4, 9/2, 5, 6, 8, 10, 14, 20, 26, 32, 40, 52\} \quad (30)$$

⁴See Refs. [52–56] for more details on the auxiliary mass flow method.

and match subsequent expansions in between where the radii of convergence overlap. In this way we find a semianalytic expression for the master integrals over the whole range of s/m^2 . In practice we do the following: We start from the expansion at $s/m^2 = -1$ where we can directly match to the numerical boundary conditions provided by `AMFlow`. From there we can move with the expansions either to smaller or larger values of s/m^2 . On the one hand, we match along the negative axis to $s/m^2 \rightarrow -\infty$ and obtain the expansion for $s/m^2 \rightarrow +\infty$ by analytic continuation. Then we match down to smaller positive values of s/m^2 until $s/m^2 = 1$. On the other hand, we move from $s/m^2 = -1$ to larger values where we stop at the two-particle threshold at $s/m^2 = 4$. We check that both ways of expanding and matching agree in the overlap region of $1 < s/m^2 < 4$ within the expected accuracy. This constitutes a non-trivial cross check on the calculation of the master integrals. We additionally cross check the expansion at $s = 0$ where a subset of master integrals have been computed analytically. Furthermore, all master integrals have been computed at $s/m^2 = 2$ and $s/m^2 = 6$ with 30 digit precision using `AMFlow` to check the results obtained through the differential equations. We find agreement within the expected uncertainty.

5.2 Calculation of master integrals for $F_{G\tilde{G}}$

Let us briefly describe the calculation for the master integrals needed for $F_{G\tilde{G}}$ at two-loop order. First, we establish a system of differential equations in the variable x defined by

$$s = -\frac{(1-x)^2}{x}. \quad (31)$$

The system of differential equations is subsequently solved with the methods described in Ref. [16]. In practice this means that we do not bring the system to canonical form, but we decouple coupled systems of differential equations into one higher-dimensional one using the package `OreSys` [57] (which is based on `Sigma` [58]) and solve this equation order-by-order in ϵ with `HarmonicSums` [59]. The largest coupled system we encounter here is a 3×3 system. For the complete solution we have to provide boundary conditions. To do this, we choose to compute the master integrals in the limit $s \rightarrow 0$ ($x \rightarrow 1$). However, since the diagrams can have cuts through only massless lines, the limit $s \rightarrow 0$ needs an asymptotic expansion. While the asymptotic expansion for some integrals can be constructed by direct integration or via simple Mellin-Barnes representations, we apply the method of regions [60] as implemented in `asy.m` [61] to the more involved master integrals. It turns out that there are three different regions, which scale as $\chi^{-0\epsilon}$, $\chi^{-2\epsilon}$ and $\chi^{-4\epsilon}$ in the variable $\chi = \sqrt{-s/m^2}$. The hard region $\propto \chi^{-0\epsilon}$ leads to massive propagators which are well studied in the literature (see, e.g., Ref. [62]). The integrals in the second region $\propto \chi^{-2\epsilon}$ can be calculated in closed form in terms of Γ functions. In the region $\propto \chi^{-4\epsilon}$ we encountered one integral which could not be calculated in terms of Γ functions. For this integral we used `HyperInt` [63] to obtain the result expanded in ϵ . It turns out that the solutions of all master integrals can be written in terms of harmonic polylogarithms [64]. We provide these results in an ancillary file [65].

The analytic results have been cross checked against numerical evaluations with FIESTA5 [66] in the euclidean region ($0 < x < 1$).

5.3 Cross checks

There are a number of checks which support the correctness of our result which we summarize in the following.

At two-loop order we reproduce the massless and massive singlet axial-vector and pseudoscalar results presented in Ref. [5]. We also agree with the one-loop corrections to $F_{G\tilde{G}}$.

Furthermore, we have performed our calculation for general QCD gauge parameter ξ and have checked that it drops out in the final result. This is a non-trivial check at three loops where ξ cancels only after including the counterterm contribution from mass renormalization.

At three loops we have cross checked the results for the massless singlet master integrals by evaluating them numerically with AMFlow [51] at $s/m^2 = 2$ and $s/m^2 = 6$. This is an important consistency check for the method which we use to compute the master integrals. We chose these points because they are separated by at least one special point like the thresholds and the high-energy expansion from our boundary conditions. Crossing these special points is the most difficult step in our approach.

A further check is the use of naive γ_5 and non-anti-commuting γ_5 for the non-singlet contributions of the axial-vector and pseudoscalar currents. Both calculations agree after taking into account the proper $\overline{\text{MS}}$ and finite renormalization constants, see Section 6.

Since our three-loop results are mainly floating point numbers, the poles also only cancel numerically against the analytically known counterterms. We can therefore use the precision of these cancellations as cross check and estimate of the uncertainty. As in Ref. [13] we define

$$\delta\left(F^{f,(3)}\Big|_{\epsilon^i}\right) = \frac{F^{(3)}\Big|_{\epsilon^i} + F^{(\text{CT}+Z)}\Big|_{\epsilon^i}}{F^{(\text{CT}+Z)}\Big|_{\epsilon^i}}, \quad (32)$$

which represents the number of correct digits for the poles of order ϵ^i . As representative examples we show the $C_F^2 T_F$ colour factor of $F_{1,\text{sing},h}^{a,f,(3)}$ and the $C_A C_F T_F$ colour factor of $F_{1,\text{sing},l}^{a,f,(3)}$ in Fig. 3.

It is clearly visible that the poles cancel with at least around 20 digits for the massive singlet and at least around 15 digits for the massless singlet contributions. In both cases we obtain this worst precision in the region $0 \leq s < 4m^2$, while it is around 30 digits over large ranges of s . Since the precision is similar or better for the other colour factors and form factors, we refrain from showing more plots.

Finally, we can explicitly check the chiral Ward identities of Eqs. (24) and (25) which relate F_1^a , F_2^a , F_p , and $F_{G\tilde{G}}$. Since they hold on the level of finite form factors, they allow

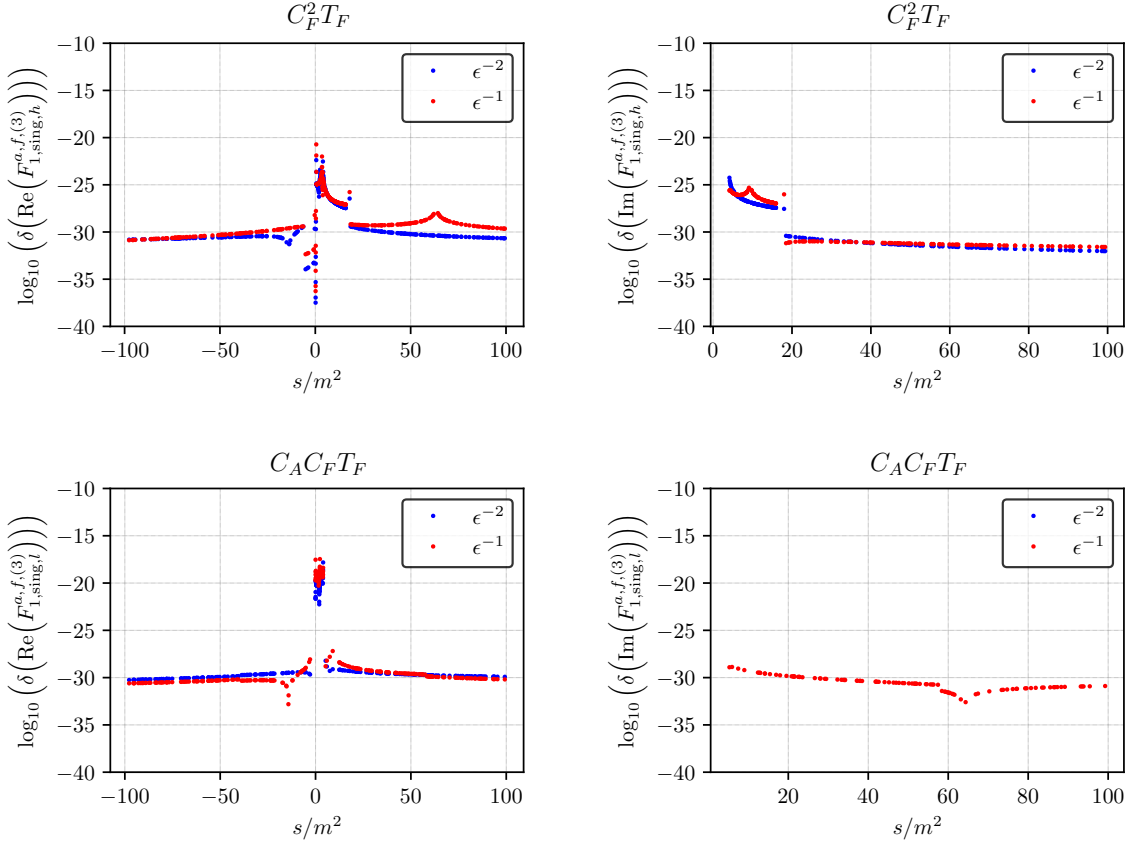


Figure 3: Relative cancellation of the poles for the $C_F^2 T_F$ colour factor of $F_{1,\text{sing},h}^{a,f,(3)}$ and the $C_A C_F T_F$ colour factor of $F_{1,\text{sing},l}^{a,f,(3)}$.

us to check their finite terms. This is especially interesting for the singlet contributions with their nontrivial renormalization including finite pieces, cf. Section 3. We define the relative precision with respect to the analytically computed $F_{G\tilde{G}}$ as

$$\delta_W(F_{\text{sing}}^{f,(3)}) = \frac{F_{1,\text{sing}}^{a,f,(3)} + \frac{s}{4m^2} F_{2,\text{sing}}^{a,f,(3)} - F_{\text{sing}}^{p,f,(3)} - \left(\frac{\alpha_s}{4\pi} T_F F_{G\tilde{G}}^f\right)^{(3)}}{\left(\frac{\alpha_s}{4\pi} T_F F_{G\tilde{G}}^f\right)^{(3)}}. \quad (33)$$

In Fig. 4 we show it for two colour factors of the massive and massless singlet contributions. The precision is similar compared to the pole cancellation discussed before and we again refrain from showing more than two representative examples.

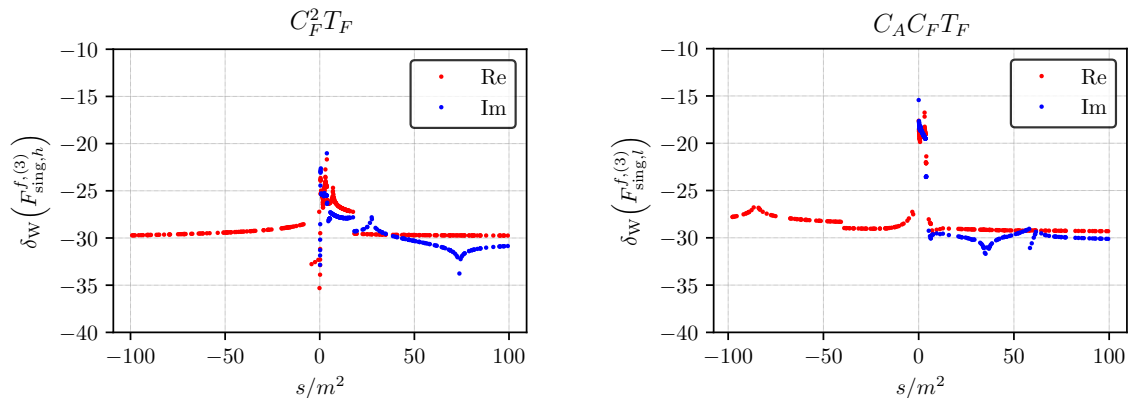


Figure 4: Precision to which the anomalous Ward identity in Eq. (25) is fulfilled for the $C_F^2 T_F$ colour factor of the massive and the $C_A C_F T_F$ colour factor for the massless singlet contributions. The quantity δ_W is defined in Eq. (33).

6 Results for the singlet form factors

In this Section we discuss our results for the singlet form factors. We present expansions for small and large values of s and for $s \rightarrow 4m^2$ and show results for the finite form factors in the whole s range. For better readability we concentrate in the main text to the contributions where the external current couples to massless quarks and relegate the formulae and plots for the massive singlet contributions to Appendix C.

We provide all results obtained in this paper as well as the non-singlet and singlet results from Refs. [12, 13] as `Mathematica` package available in Ref. [67]. Furthermore we implemented these results in the `Fortran` library `FF31` available in Ref. [68] which allows for a fast numerical evaluation of all form factors. The library is described in more detail in Appendix E.

6.1 Comparison of naive and Larin γ_5 prescription for axial-vector and pseudoscalar non-singlet form factors

It is interesting to discuss the tree-level results for the two γ_5 prescriptions. For the axial-vector and pseudoscalar current we find

$$\begin{aligned}
 F_{1,\text{naive}}^{a,(0)} &= 1, \\
 F_{2,\text{naive}}^{a,(0)} &= 0, \\
 F_{1,\text{larin}}^{a,(0)} &= 1 - \epsilon \frac{32m^2 - 5s}{3(4m^2 - s)} + \epsilon^2 \frac{4(4m^2 + s)}{3(4m^2 - s)} - \epsilon^3 \frac{4s}{3(4m^2 - s)},
 \end{aligned}$$

$$\begin{aligned}
F_{2,\text{larin}}^{a,(0)} &= -\epsilon \frac{8m^2(2m^2 - s)}{s(4m^2 - s)} + \epsilon^2 \frac{64m^2(2m^2 - s)}{3s(4m^2 - s)} - \epsilon^3 \frac{32m^2(2m^2 - s)}{3s(4m^2 - s)}, \\
F_{\text{naive}}^{p,(0)} &= 1, \\
F_{\text{larin}}^{p,(0)} &= 1 - \epsilon \frac{12m^2 + 19s}{6s} + \epsilon^2 \frac{44m^2 + 13s}{6s} - \epsilon^3 \frac{2(12m^2 - s)}{3s} + \epsilon^4 \frac{2(4m^2 - s)}{3s}, \quad (34)
\end{aligned}$$

with our choice of projectors, cf. Appendix A. Note that there is a non-trivial s dependence at higher orders in ϵ . Through renormalization of the quark wave function and the subtraction of infrared divergences they induce finite terms in ϵ at one-loop order. At two and three loops even poles are generated which are important to obtain finite expressions for the form factors.

We have used the prescription of Ref. [25] for γ_5 also for the one-, two-, and three-loop form factors. After renormalization and infrared subtraction we obtain

$$\begin{aligned}
F_{1,\text{naive}}^{a,(i),f} &= F_{1,\text{larin}}^{a,(i),f}, \\
F_{2,\text{naive}}^{a,(i),f} &= F_{2,\text{larin}}^{a,(i),f}, \\
F_{\text{naive}}^{p,(i),f} &= F_{\text{larin}}^{p,(i),f}, \quad (35)
\end{aligned}$$

for $i = 1, 2, 3$. Let us stress that it is important to thoroughly follow the instructions from Section 3 and take into account all relevant renormalization constants from Appendix B.

6.2 Expansions for $s \rightarrow 0$, $s \rightarrow -\infty$, and $s \rightarrow 4m^2$

In this Section we concentrate on the singlet contributions and present explicit results for the expansions for small and large values of s and close to threshold. We choose $\mu^2 = m^2$ for the renormalization scale. For completeness we present both two- and three-loop expressions.

Including terms up to linear order in $\chi = \sqrt{-s/m^2}$ we obtain for the massless singlet contribution in the limit $s \rightarrow 0$

$$F_{1,\text{sing},l}^{v,f} \Big|_{s \rightarrow 0} = \left(\frac{\alpha_s}{\pi} \right)^3 \frac{d_{abc} d^{abc}}{N_C} [-0.64927 + 0.99711\chi], \quad (36)$$

$$F_{2,\text{sing},l}^{v,f} \Big|_{s \rightarrow 0} = \left(\frac{\alpha_s}{\pi} \right)^3 \frac{d_{abc} d^{abc}}{N_C} [-5.7080 - 6.5797 \ln(\chi) + \chi(8.1838 - 3.7011 \ln(\chi))], \quad (37)$$

$$\begin{aligned}
F_{1,\text{sing},l}^{a,f} \Big|_{s \rightarrow 0} &= \left(\frac{\alpha_s}{\pi} \right)^2 C_F T_F \left[-\frac{7}{4} + \frac{\pi^2}{4} \chi \right] \\
&+ \left(\frac{\alpha_s}{\pi} \right)^3 C_F T_F \left[C_F \left(-1.4887 + 1.2337\chi \right) + C_A \left(-9.0185 + \chi(6.3166 - 7.8134 \ln(\chi)) \right) \right] \\
&+ T_F n_h \left(-0.32519 \right) + T_F n_l \left(3.6797 + \chi(-1.4751 + 3.2899 \ln(\chi)) \right) \Big], \quad (38)
\end{aligned}$$

$$\begin{aligned}
F_{2,\text{sing},l}^{a,f} \Big|_{s \rightarrow 0} &= \left(\frac{\alpha_s}{\pi}\right)^2 C_F T_F \left[\frac{\pi^2}{2\chi} - \frac{2}{3} \ln^2(\chi) + \frac{25}{9} \ln(\chi) - \frac{95}{54} - \frac{\pi^2}{9} \right] \\
&+ \left(\frac{\alpha_s}{\pi}\right)^3 C_F T_F \left[C_F \left(\frac{2.4674}{\chi} + 6.3840 \ln(\chi) + 2.2099 + \chi(2.8786 \ln(\chi) - 5.0719) \right) \right. \\
&+ C_A \left(-\frac{15.627 \ln(\chi) + 5.3408}{\chi} + 0.81481 \ln^3(\chi) - 2.6308 \ln^2(\chi) + 4.2083 \ln(\chi) \right. \\
&+ 14.089 + \chi(6.0657 \ln(\chi) - 5.3476) \left. \right) + T_F n_h \left(-0.96834 \ln(\chi) + 0.15303 + 0.90471 \chi \right) \\
&+ T_F n_l \left(\frac{6.5797 \ln(\chi) + 4.5177}{\chi} - 0.29630 \ln^3(\chi) + 1.2593 \ln^2(\chi) + 0.47451 \ln(\chi) \right. \\
&\left. \left. - 5.9964 + \chi(-2.4674 \ln(\chi) - 0.049185) \right) \right], \tag{39}
\end{aligned}$$

where terms of $\mathcal{O}(\chi^2)$ have been neglected and the analytic continuation for $s > 0$ is given by $\chi = \sqrt{-s/m^2} = -i\sqrt{s/m^2}$. The results for the massive singlet form factors can be found in Eq. (56). It is interesting to note that the axial-vector form factor $F_{2,\text{sing},l}^{a,f}$ develops $1/\sqrt{-s/m^2}$ terms, both at two and three loops, which are absent in the massive case. $F_{2,\text{sing},l}^{a,f}$ also has logarithmic contributions up to third order in the $(s/m^2)^0$ term whereas $F_{2,\text{sing},l}^{v,f}$ only has linear logarithms. $F_{1,\text{sing},l}^{a,f}$ starts to develop logarithms at order $\sqrt{-s/m^2}$ and the vector contribution $F_{1,\text{sing},l}^{v,f}$ only at order s/m^2 .

In the high-energy limit the expansions of the massless singlet form factors are given by

$$\begin{aligned}
F_{1,\text{sing},l}^{v,f} \Big|_{s \rightarrow -\infty} &= \left(\frac{\alpha_s}{\pi}\right)^3 \left[-0.334349 + \frac{m^2}{-s} \left(-0.00833333l_s^5 - 0.116245l_s^4 - 0.639133l_s^3 \right. \right. \\
&\left. \left. - 0.484656l_s^2 + 13.7669l_s + 46.9765 \right) \right], \tag{40}
\end{aligned}$$

$$F_{2,\text{sing},l}^{v,f} \Big|_{s \rightarrow -\infty} = \left(\frac{\alpha_s}{\pi}\right)^3 \frac{m^2}{-s} \left[-4.57974l_s - 7.34102 \right], \tag{41}$$

$$\begin{aligned}
F_{1,\text{sing},l}^{a,f} \Big|_{s \rightarrow -\infty} &= \left(\frac{\alpha_s}{\pi}\right)^2 C_F T_F \left[-\frac{3}{4}l_s - \frac{9}{4} + \frac{\pi^2}{12} + \frac{m^2}{-s} \left\{ \frac{1}{2}l_s^2 + \frac{3}{2}l_s + \frac{1}{2} + \frac{\pi^2}{2} \right\} \right] \\
&+ \left(\frac{\alpha_s}{\pi}\right)^3 C_F T_F \left[C_F \left(0.1875l_s^3 + 0.919383l_s^2 + 1.7663l_s + 0.520574 \right) \right. \\
&+ C_A \left(-0.6875l_s^2 - 4.09631l_s - 6.70052 \right) + T_F n_h \left(0.25l_s^2 + 1.03502l_s + 2.34309 \right) \\
&+ T_F n_l \left(0.25l_s^2 + 1.03502l_s + 2.34309 \right) + \frac{m^2}{-s} \left\{ C_F \left(-0.0833333l_s^4 - 0.529589l_s^3 \right. \right. \\
&\left. \left. - 5.50593l_s^2 - 17.2508l_s - 32.6278 \right) + C_A \left(-0.00208333l_s^5 - 0.0751055l_s^4 + 0.141666l_s^3 \right. \right. \\
&\left. \left. + 3.33973l_s^2 + 15.0217l_s + 36.7552 \right) + T_F n_h \left(-0.166667l_s^3 - 1.59058l_s^2 - 3.29888l_s \right. \right.
\end{aligned}$$

$$- 7.38784) + T_F n_l \left(-0.166667 l_s^3 - 1.09058 l_s^2 - 3.50612 l_s - 6.4258 \right) \Big] \Big\}, \quad (42)$$

$$\begin{aligned} F_{2,\text{sing},l}^{a,f} \Big|_{s \rightarrow -\infty} &= \left(\frac{\alpha_s}{\pi} \right)^2 C_F T_F \frac{m^2}{-s} \left[-\frac{1}{2} l_s^2 - 3 l_s - 2 - \frac{\pi^2}{3} \right] \\ &+ \left(\frac{\alpha_s}{\pi} \right)^3 C_F T_F \frac{m^2}{-s} \left[C_F \left(0.104167 l_s^4 + 1. l_s^3 + 6.68117 l_s^2 + 22.4839 l_s + 34.67 \right) \right. \\ &+ C_A \left(0.0208333 l_s^4 - 0.611111 l_s^3 - 7.80858 l_s^2 - 30.0535 l_s - 49.2293 \right) \\ &+ T_F n_h \left(0.222222 l_s^3 + 2.05556 l_s^2 + 6.33333 l_s + 8.54753 \right) \\ &\left. + T_F n_l \left(0.222222 l_s^3 + 2.05556 l_s^2 + 6.33333 l_s + 10.147 \right) \right], \quad (43) \end{aligned}$$

where $l_s = \log(m^2/(-s - i\delta))$ and we neglect terms which are suppressed by m^4/s^2 . In the leading term there are at most cubic logarithms which are present for $F_{1,\text{sing},l}^{a,f}$. In the subleading term l_s^5 terms appear for $F_{1,\text{sing},l}^{a,f}$ and $F_{1,\text{sing},l}^{v,f}$ whereas the leading logarithm for $F_{2,\text{sing},l}^{a,f}$ is l_s^4 and $F_{2,\text{sing},l}^{v,f}$ only has linear subleading logarithms. The corresponding results for the massive singlet form factors can be found in Eq. (62).

For some of the coefficients in the high-energy expansion our method provides a numerical accuracy of several ten digits for the massless and several hundred digits for the massive singlet contributions. The accuracy for the massless contributions is of course limited by the numerical boundary conditions while we have analytic boundary conditions for the massive contributions. The high accuracy allows for the application of the PSLQ algorithm [69] to reconstruct the analytic expressions. For example we find

$$\begin{aligned} F_{1,\text{sing},l}^{a,f,(3)} \Big|_{m^0/(-s)^0, l_s^3} &= \frac{3C_F^2 T_F}{16}, \\ F_{1,\text{sing},l}^{a,f,(3)} \Big|_{m^0/(-s)^0, l_s^2} &= C_F^2 T_F \left(\frac{9}{8} - \frac{\pi^2}{48} \right) - \frac{11C_A C_F T_F}{16} + \frac{C_F T_F^2 n_h}{4} + \frac{C_F T_F^2 n_l}{4} \end{aligned} \quad (44)$$

for the leading and subleading logarithms of $F_{1,\text{sing},l}^{a,f,(3)}$.

Close to threshold it is convenient to parameterize the form factors in terms of the velocity of the produced quarks, $\beta = \sqrt{1 - 4m^2/s}$. We observe that the two-loop and the three-loop vector corrections start with β^0 . The three-loop axial-vector form factors develop $1/\beta$ terms which read

$$F_{1,\text{sing},l}^{a,f} \Big|_{s \rightarrow 4m^2} = \left(\frac{\alpha_s}{\pi} \right)^3 C_F^2 T_F \frac{1}{\beta} \left[(2.6544 - 0.4750i) l_{2\beta} - 3.4005 - 3.6946i \right], \quad (45)$$

$$F_{2,\text{sing},l}^{a,f} \Big|_{s \rightarrow 4m^2} = \left(\frac{\alpha_s}{\pi} \right)^3 C_F^2 T_F \frac{1}{\beta} \left[-(0.18704 + 1.18515i) l_{2\beta} + 0.79281 - 0.18115i \right], \quad (46)$$

where $l_{2\beta} = \log(2\beta)$. The $1/\beta$ terms for the massive singlet form factors are provided in Eq. (66).

6.3 Finite form factors

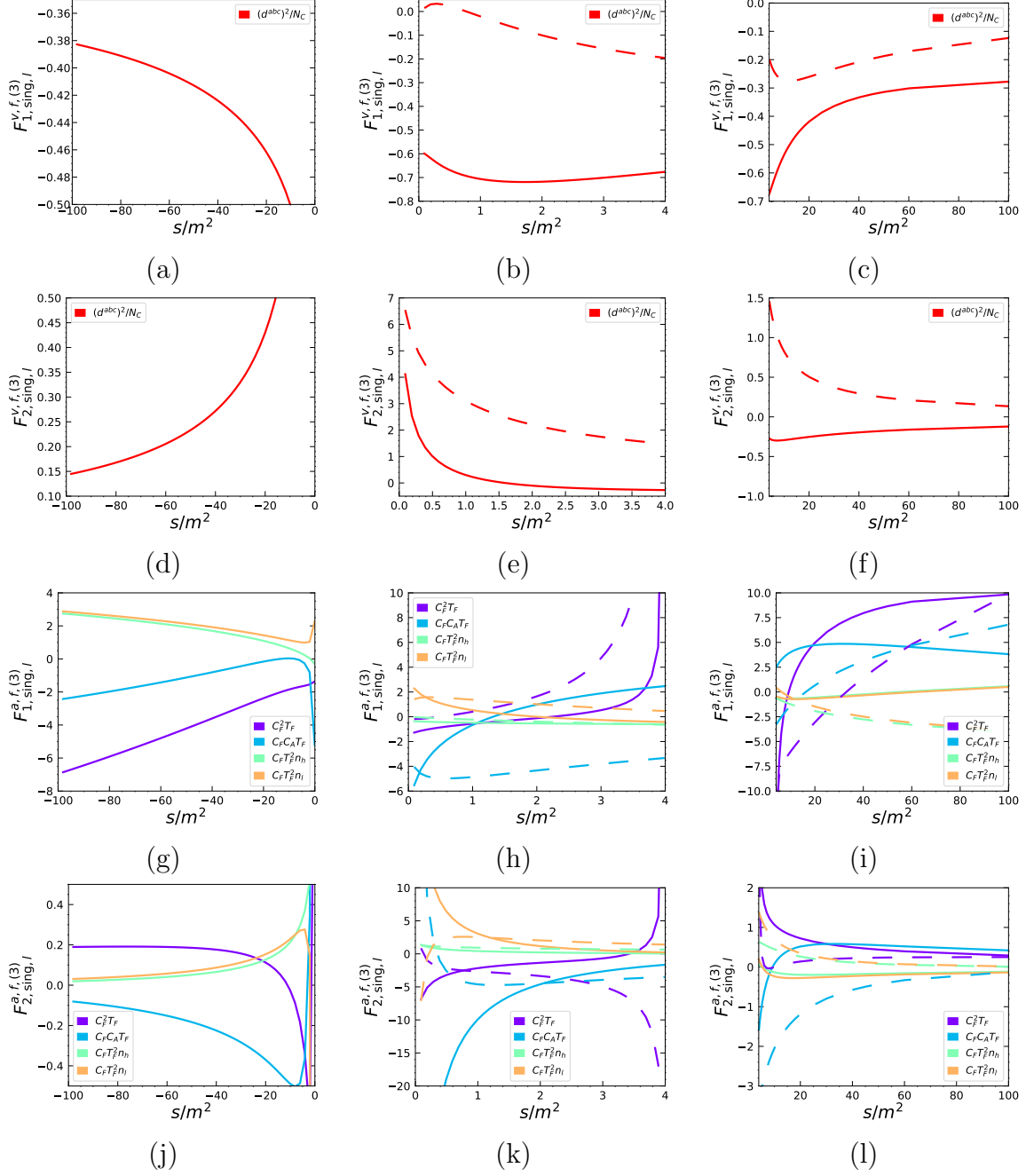


Figure 5: Massless singlet form factors as a function of s for $\mu^2 = m^2$.

In Fig. 5 we show the finite results for the massless singlet form factors as a function of s . We subdivide the energy range into three parts corresponding to negative values of s , the region between $s = 0$ and the threshold $s = 4m^2$, and above threshold and show results

for all individual colour factors. We present both real (solid) and imaginary (dashed) parts. In contrast to the non-singlet contributions the singlet form factors develop an imaginary part also for $s \in [0, 4m^2]$ since there are cuts through the gluons and in the massless singlet case in addition through the massless quarks. One recognizes the strong power-like divergences for $s \rightarrow 0$ and $s \rightarrow 4m^2$ which are present in some of the form factors. On the other hand, the logarithmic divergences in the various limits exhibit only a mild behaviour.

7 Conclusions

The main result of this paper are the three-loop corrections to the singlet form factors with massive external quarks where external vector, axial-vector, scalar, or pseudoscalar currents couple to a closed massless or massive quark loop. This complements the non-singlet and massive singlet contributions presented in Refs. [12,13]. We present our results in an easy-to-use form as `Mathematica` package and `Fortran` library with high numerical precision in the whole s range. Our method allows for a systematic improvement of the accuracy if needed.

For the computation of the master integrals we use the “expand and match” approach which has been introduced in Ref. [49] and further developed in Refs. [12,13]. It provides analytic expansions with numerical coefficients for all master integrals around properly chosen kinematic points leading to precise results for the form factors in the respective energy region. In the paper we provide expansions around the physically interesting points $s \rightarrow 0$, $s \rightarrow -\infty$ and $s \rightarrow 4m^2$. In some cases the numerical precision is sufficiently high such that the analytic result of the expansion coefficients can be reconstructed.

In the course of our calculation we obtained a number of further interesting results. For example, we have applied two different prescriptions for the treatment of γ_5 to the non-singlet axial-vector and pseudoscalar form factors and have checked by an explicit calculation that the final finite expressions are identical. Furthermore, we have computed analytic two-loop corrections to the massive pseudoscalar-gluon-heavy-quark vertex which we needed to check the non-renormalization of the Adler-Bell-Jackiw anomaly at three-loop order.

Acknowledgments

This research was supported by the Deutsche Forschungsgemeinschaft (DFG, German Research Foundation) under grant 396021762 — TRR 257 “Particle Physics Phenomenology after the Higgs Discovery” and by the European Research Council (ERC) under the European Union’s Horizon 2020 research and innovation programme grant agreement 101019620 (ERC Advanced Grant TOPUP). The work of M.F. was supported in part by

the European Union’s Horizon 2020 research and innovation program under the Marie Skłodowska-Curie grant agreement No. 101065445 – PHOBIDE. The Feynman diagrams were drawn with the help of Axodraw [70] and JaxoDraw [71].

A Projectors

To project onto the form factors given by Eq. (2) we define the projectors

$$F_i = \text{Tr}[P_i^\mu(q_2 + m)\Gamma_{i,\mu}(q_1 + m)] \quad (47)$$

with

$$\begin{aligned} P_1^{v,\mu} &= \frac{(4m^2 - s)\gamma^\mu - 2(3 - 2\epsilon)m(q_1^\mu + q_2^\mu)}{4(-1 + \epsilon)(4m^2 - s)^2}, \\ P_2^{v,\mu} &= \frac{-m^2(4m^2 - s)\gamma^\mu + (2m^2 + s - \epsilon s)m(q_1^\mu + q_2^\mu)}{(-1 + \epsilon)(4m^2 - s)^2 s}, \\ P_1^{a,\mu} &= \frac{s\gamma^\mu\gamma_5 - 2m\gamma_5(q_1^\mu - q_2^\mu)}{4(-1 + \epsilon)(4m^2 - s)s}, \\ P_2^{a,\mu} &= \frac{-sm^2\gamma^\mu\gamma_5 + (6m^2 - 4\epsilon m^2 - s + \epsilon s)m\gamma_5(q_1^\mu - q_2^\mu)}{(-1 + \epsilon)(4m^2 - s)s^2}, \\ P^{s,\mu} &= \frac{1}{2m(4m^2 - s)}, \\ P^{p,\mu} &= -i\frac{\gamma_5}{2ms}. \end{aligned} \quad (48)$$

γ_5 is replaced using Eq. (5).

B Renormalization constants

In our calculation there are several (non-standard) renormalization constants which are needed due to the use of non-anti-commuting γ_5 . For convenience of the reader we reproduce all of them in the following. We use the notion for “singlet” and “non-singlet” as defined in Section 1.

For the axial-vector contribution we need [24, 25]

$$\begin{aligned} Z_{a,S}^{\overline{\text{MS}}} &= 1 + \left(\frac{\alpha_s}{\pi}\right)^2 \frac{1}{\epsilon} \left(\frac{11}{24} C_A C_F + \frac{5}{24} C_F n_f T_F \right) + \left(\frac{\alpha_s}{\pi}\right)^3 \left(\frac{1}{\epsilon^2} \left[-\frac{121}{432} C_A^2 C_F \right. \right. \\ &\quad \left. \left. - \frac{11}{432} C_A C_F T_F n_f + \frac{5}{108} C_F T_F^2 n_f^2 \right] + \frac{1}{\epsilon} \left[-\frac{77}{144} C_A C_F^2 + \frac{1789}{2592} C_A^2 C_F \right. \right. \\ &\quad \left. \left. + \frac{149}{2592} C_A C_F T_F n_f - \frac{11}{144} C_F^2 T_F n_f + \frac{13}{648} C_F T_F^2 n_f^2 \right] \right) + \mathcal{O}(\alpha_s^4), \end{aligned}$$

$$\begin{aligned}
Z_{a,\text{NS}}^{\overline{\text{MS}}} &= 1 + \left(\frac{\alpha_s}{\pi}\right)^2 \frac{1}{\epsilon} \left(\frac{11}{24} C_A C_F - \frac{1}{6} C_F T_F n_f \right) + \left(\frac{\alpha_s}{\pi}\right)^3 \left(\frac{1}{\epsilon^2} \left[-\frac{121}{432} C_A^2 C_F \right. \right. \\
&\quad \left. \left. + \frac{11}{54} C_A C_F T_F n_f - \frac{1}{27} C_F T_F^2 n_f^2 \right] + \frac{1}{\epsilon} \left[-\frac{77}{144} C_A C_F^2 - \frac{26}{81} C_A C_F T_F n_f \right. \right. \\
&\quad \left. \left. + \frac{1789}{2592} C_A^2 C_F + \frac{1}{9} C_F^2 T_F n_f + \frac{1}{162} C_F T_F^2 n_f^2 \right] \right) + \mathcal{O}(\alpha_s^4), \\
Z_{a,\text{S}}^{\text{fin}} &= 1 - \frac{\alpha_s}{\pi} C_F + \left(\frac{\alpha_s}{\pi}\right)^2 \left(-\frac{107}{144} C_A C_F + \frac{11}{8} C_F^2 + \frac{31}{144} C_F T_F n_f \right) \\
&\quad + \left(\frac{\alpha_s}{\pi}\right)^3 \left(\left[\frac{55\zeta_3}{48} - \frac{133}{2592} \right] C_A C_F T_F n_f + \left[\frac{2917}{864} - \frac{5\zeta_3}{2} \right] C_A C_F^2 \right. \\
&\quad \left. + \left[\frac{7\zeta_3}{8} - \frac{2147}{1728} \right] C_A^2 C_F + \left[\frac{497}{1728} - \frac{13\zeta_3}{12} \right] C_F^2 T_F n_f + \frac{79}{324} C_F n_f^2 T_F^2 \right. \\
&\quad \left. + \left[\frac{3\zeta_3}{2} - \frac{185}{96} \right] C_F^3 \right) + \mathcal{O}(\alpha_s^4), \\
Z_{a,\text{NS}}^{\text{fin}} &= 1 - \frac{\alpha_s}{\pi} C_F + \left(\frac{\alpha_s}{\pi}\right)^2 \left(-\frac{107}{144} C_A C_F + \frac{11}{8} C_F^2 + \frac{1}{36} C_F T_F n_f \right) \\
&\quad + \left(\frac{\alpha_s}{\pi}\right)^3 \left(\left[\frac{2917}{864} - \frac{5}{2} \zeta_3 \right] C_A C_F^2 + \left[\frac{89}{648} + \frac{\zeta_3}{3} \right] C_A C_F T_F n_f + \left[-\frac{2147}{1728} \right. \right. \\
&\quad \left. \left. + \frac{7}{8} \zeta_3 \right] C_A^2 C_F + \left[-\frac{185}{96} + \frac{3}{2} \zeta_3 \right] C_F^3 + \left[-\frac{31}{432} - \frac{1}{3} \zeta_3 \right] C_F^2 T_F n_f \right. \\
&\quad \left. + \frac{13}{324} C_F T_F^2 n_f^2 \right) + \mathcal{O}(\alpha_s^4). \tag{49}
\end{aligned}$$

$Z_{a,\text{S}}^{\overline{\text{MS}}}$ is taken from Eq. (19) of the arXiv version of Ref. [25] and $Z_{a,\text{S}}^{\text{fin}}$ from Eq. (5.4) of Ref. [35]. $Z_{a,\text{NS}}^{\overline{\text{MS}}}$ and $Z_{a,\text{NS}}^{\text{fin}}$ are obtained from Eqs. (8) and (11) of Ref. [24].

For the pseudoscalar contribution we have

$$\begin{aligned}
Z_p^{\overline{\text{MS}}} &= 1 - \frac{\alpha_s}{\pi} \frac{3C_F}{4\epsilon} + \left(\frac{\alpha_s}{\pi}\right)^2 \left(\frac{1}{\epsilon^2} \left[\frac{11}{32} C_A C_F + \frac{9}{32} C_F^2 - \frac{1}{8} C_F T_F n_f \right] + \frac{1}{\epsilon} \left[\frac{79}{192} C_A C_F \right. \right. \\
&\quad \left. \left. - \frac{3}{64} C_F^2 - \frac{11}{48} C_F T_F n_f \right] \right) + \left(\frac{\alpha_s}{\pi}\right)^3 \left(\frac{1}{\epsilon^3} \left[-\frac{33}{128} C_A C_F^2 + \frac{11}{72} C_A C_F T_F n_f \right. \right. \\
&\quad \left. \left. - \frac{121}{576} C_A^2 C_F - \frac{9}{128} C_F^3 + \frac{3}{32} C_F^2 T_F n_f - \frac{1}{36} C_F T_F^2 n_f^2 \right] + \frac{1}{\epsilon^2} \left[-\frac{215}{768} C_A C_F^2 \right. \right. \\
&\quad \left. \left. + \frac{55}{432} C_A C_F T_F n_f - \frac{257}{3456} C_A^2 C_F + \frac{9}{256} C_F^3 + \frac{19}{192} C_F^2 T_F n_f - \frac{11}{216} C_F T_F^2 n_f^2 \right] \right. \\
&\quad \left. + \frac{1}{\epsilon} \left[\frac{3203}{2304} C_A C_F^2 + \left(-\frac{29}{144} + \frac{1}{4} \zeta_3 \right) C_A C_F n_f T_F - \frac{599}{6912} C_A^2 C_F - \frac{43}{128} C_F^3 \right. \right. \\
&\quad \left. \left. + \left(-\frac{107}{288} - \frac{1}{4} \zeta_3 \right) C_F^2 T_F n_f + \frac{17}{432} C_F T_F^2 n_f^2 \right] \right) + \mathcal{O}(\alpha_s^4),
\end{aligned}$$

$$\begin{aligned}
Z_p^{\text{fin}} = & 1 - 2\frac{\alpha_s}{\pi}C_F + \left(\frac{\alpha_s}{\pi}\right)^2 \left(\frac{1}{72}C_A C_F + \frac{1}{18}C_F T_F n_f\right) + \left(\frac{\alpha_s}{\pi}\right)^3 \left(\left[-\frac{25}{54}\right.\right. \\
& + \left.\frac{19}{2}\zeta_3\right]C_A C_F^2 + \left[\frac{107}{324} + \frac{2}{3}\zeta_3\right]C_A C_F T_F n_f + \left[-\frac{479}{864} - \frac{13}{4}\zeta_3\right]C_A^2 C_F \\
& \left. + \left[\frac{19}{12} - 6\zeta_3\right]C_F^3 + \left[-\frac{145}{216} - \frac{2}{3}\zeta_3\right]C_F^2 T_F n_f + \frac{13}{162}C_F T_F^2 n_f^2\right) + \mathcal{O}(\alpha_s^4), \quad (50)
\end{aligned}$$

which corresponds to Eqs. (13) and (15) of the arXiv version of Ref. [25].

Note that $Z_p^{\overline{\text{MS}}}$ is the renormalization constant associated to the factor m on the r.h.s. of j^p in Eq. (1). It replaces the usual $\overline{\text{MS}}$ renormalization constant $Z_m^{\overline{\text{MS}}}$ for the heavy-quark mass which is used for anti-commuting γ_5 , e.g. for the non-singlet contribution. In case only the singlet contribution is considered only the $\mathcal{O}(\alpha_s)$ terms are needed from $Z_p^{\overline{\text{MS}}}$. Up to this order $Z_p^{\overline{\text{MS}}}$ agrees with $Z_m^{\overline{\text{MS}}}$. Note that in Ref. [13] the factor m in Eq. (1) has been renormalized on-shell.

We refrain from providing explicit expressions for the wave function, strong coupling constant, and heavy-quark mass renormalization constants, which have already been used in Refs. [12, 13].

C Results for the massive singlet contribution

In this Section we collect the expansions around $s = 0$, around the threshold $s = 4m^2$, and in the high-energy limit for the massive singlet contributions in the spirit of those for the massless singlet contributions shown in Subsection 6.2. We also show plots over the whole range of s .

In the limit $s \rightarrow 0$ we obtain for the six form factors

$$F_{1,\text{sing},h}^{v,f} \Big|_{s \rightarrow 0} = 0, \quad (51)$$

$$F_{2,\text{sing},h}^{v,f} \Big|_{s \rightarrow 0} = \left(\frac{\alpha_s}{\pi}\right)^3 \frac{d_{abc}d^{abc}}{n_c} [0.371005], \quad (52)$$

$$\begin{aligned}
F_{1,\text{sing},h}^{a,f} \Big|_{s \rightarrow 0} = & \left(\frac{\alpha_s}{\pi}\right)^2 C_F T_F \left[-\frac{19}{12} + \frac{2}{9}\pi^2\right] \\
& + \left(\frac{\alpha_s}{\pi}\right)^3 C_F T_F \left[0.79884C_A - 4.3999C_F + 0.66880T_F n_h + 1.2009T_F n_l\right], \quad (53)
\end{aligned}$$

$$\begin{aligned}
F_{2,\text{sing},h}^{a,f} \Big|_{s \rightarrow 0} = & \left(\frac{\alpha_s}{\pi}\right)^2 C_F T_F \left[\frac{2}{3} + \frac{1}{90}\pi^2 - \frac{1}{24}\pi^2\chi\right] \\
& + \left(\frac{\alpha_s}{\pi}\right)^3 C_F T_F \left[2.4737C_A + 3.1457C_F + 0.36848T_F n_h - 0.73194T_F n_l\right]
\end{aligned}$$

$$+ \chi \left\{ C_A(1.3022 \ln(\chi) - 2.2422) - 1.8506C_F + T_F n_l(-0.54831 \ln(\chi) + 0.86816) \right\} \Bigg], \quad (54)$$

$$F_{\text{sing},h}^{s,f} \Big|_{s \rightarrow 0} = \left(\frac{\alpha_s}{\pi} \right)^2 C_F T_F \left[-2 + \frac{1}{3} \pi^2 - \frac{1}{12} \pi^2 \chi \right] \\ + \left(\frac{\alpha_s}{\pi} \right)^3 C_F T_F \left[7.2423 C_A - 2.1288 C_F + 0.47311 T_F n_h - 1.4332 T_F n_l \right. \\ \left. + \chi (C_A(3.0157 \ln(\chi) - 4.6557) - 0.20562 C_F + T_F n_l(-1.0966 \ln(\chi) + 1.4622)) \right], \quad (55)$$

$$F_{\text{sing},h}^{p,f} \Big|_{s \rightarrow 0} = \left(\frac{\alpha_s}{\pi} \right)^2 C_F T_F \left[\frac{1}{6} + \frac{2}{9} \pi^2 - \frac{1}{8} \pi^2 \chi \right] \\ + \left(\frac{\alpha_s}{\pi} \right)^3 C_F T_F \left[+9.8173 C_A - 0.55128 C_F + 0.99399 T_F n_h - 2.4788 T_F n_l \right. \\ \left. + \chi (C_A(3.9067 \ln(\chi) - 7.6518) - 1.8506 C_F + T_F n_l(-1.6449 \ln(\chi) + 2.6045)) \right], \quad (56)$$

where again terms of $\mathcal{O}(\chi^2)$ have been neglected. Logarithmic contributions appear only at order $\chi = \sqrt{-s/m^2}$ and thus the limit $s = 0$ exists for all form factors.

In the high-energy limit we have

$$F_{1,\text{sing},h}^{v,f} \Big|_{s \rightarrow -\infty} = \left(\frac{\alpha_s}{\pi} \right)^3 \frac{d_{abc} d^{abc}}{n_c} \left[-0.33435 + \frac{m^2}{-s} (-0.00833333 l_s^5 - 0.11624 l_s^4 \right. \\ \left. - 0.63913 l_s^3 - 0.83260 l_s^2 + 15.749 l_s + 66.917) \right], \quad (57)$$

$$F_{2,\text{sing},h}^{v,f} \Big|_{s \rightarrow -\infty} = \left(\frac{\alpha_s}{\pi} \right)^3 \frac{d_{abc} d^{abc}}{n_c} \left[\frac{m^2}{-s} (-4.5797 l_s - 7.3410) \right], \quad (58)$$

$$F_{1,\text{sing},h}^{a,f} \Big|_{s \rightarrow -\infty} = \left(\frac{\alpha_s}{\pi} \right)^2 C_F T_F \left[-\frac{3}{4} l_s - \frac{9}{4} + \frac{\pi^2}{12} + \frac{m^2}{-s} \left\{ \frac{1}{2} l_s^2 + \left(\frac{3}{2} - \frac{\pi^2}{3} \right) l_s + \frac{1}{2} - \frac{\pi^2}{2} + 4\zeta_3 \right\} \right] \\ + \left(\frac{\alpha_s}{\pi} \right)^3 C_F T_F \left[C_F \left(0.18750 l_s^3 + 0.91938 l_s^2 + 1.7663 l_s + 0.52057 \right) \right. \\ + C_A \left(-0.68750 l_s^2 - 4.0963 l_s - 6.7005 \right) + T_F n_h \left(0.25000 l_s^2 + 1.0350 l_s + 2.3431 \right) \\ + T_F n_l \left(0.25000 l_s^2 + 1.0350 l_s + 2.3431 \right) + \frac{m^2}{-s} \left\{ C_F \left(-0.0833333 l_s^4 + 0.29288 l_s^3 \right. \right. \\ \left. \left. - 3.2283 l_s^2 - 0.27409 l_s + 2.5837 \right) + C_A \left(-0.00208333 l_s^5 - 0.075106 l_s^4 + 0.14167 l_s^3 \right. \right. \\ \left. \left. - 0.48000 l_s^2 - 6.8168 l_s + 9.9023 \right) + T_F n_h \left(-0.16667 l_s^3 + 0.054357 l_s^2 \right. \right. \\ \left. \left. + 3.1403 l_s + 6.4236 \right) + T_F n_l \left(-0.16667 l_s^3 + 0.55436 l_s^2 + 2.9330 l_s + 5.7888 \right) \right\} \Bigg], \quad (59)$$

$$\begin{aligned}
F_{2,\text{sing},h}^{a,f} \Big|_{s \rightarrow -\infty} &= \left(\frac{\alpha_s}{\pi}\right)^2 C_F T_F \frac{m^2}{-s} \left[-\frac{1}{2} l_s^2 - 3l_s - 2 - \frac{\pi^2}{3} \right] \\
&+ \left(\frac{\alpha_s}{\pi}\right)^3 C_F T_F \frac{m^2}{-s} \left[C_F \left(0.10417l_s^4 + 1.0000l_s^3 + 6.6812l_s^2 + 22.484l_s + 34.670 \right) \right. \\
&+ C_A \left(0.020833l_s^4 - 0.61111l_s^3 - 7.8086l_s^2 - 30.054l_s - 49.229 \right) \\
&+ T_F n_h \left(0.22222l_s^3 + 2.0556l_s^2 + 6.3333l_s + 8.5475 \right) \\
&\left. + T_F n_l \left(0.22222l_s^3 + 2.0556l_s^2 + 6.3333l_s + 10.147 \right) \right], \tag{60}
\end{aligned}$$

$$\begin{aligned}
F_{\text{sing},h}^{s,f} \Big|_{s \rightarrow -\infty} &= \left(\frac{\alpha_s}{\pi}\right)^2 C_F T_F \left[-\frac{1}{48} l_s^4 + \left(1 - \frac{\pi^2}{12}\right) l_s^2 + (4 - 3\zeta_3) l_s + \frac{2\pi^2}{3} - \frac{\pi^4}{45} \right] \\
&+ \left(\frac{\alpha_s}{\pi}\right)^3 C_F T_F \frac{m^2}{-s} \left[C_F \left(0.0041667l_s^6 - 0.0062500l_s^5 + 0.062124l_s^4 + 1.0817l_s^3 + 4.8496l_s^2 \right. \right. \\
&+ 32.500l_s + 58.066 \left. \right) + C_A \left(0.0010417l_s^6 - 0.022917l_s^5 - 0.14492l_s^4 + 0.46401l_s^3 \right. \\
&+ 3.6270l_s^2 + 9.0468l_s + 16.307 \left. \right) + T_F n_h \left(0.0083333l_s^5 + 0.023148l_s^4 - 0.078904l_s^3 \right. \\
&- 0.31219l_s^2 - 2.1741l_s - 1.2446 \left. \right) + T_F n_l \left(0.0083333l_s^5 + 0.023148l_s^4 - 0.078904l_s^3 \right. \\
&\left. - 0.31219l_s^2 - 3.8614l_s - 6.4797 \right) \left. \right], \tag{61}
\end{aligned}$$

$$\begin{aligned}
F_{\text{sing},h}^{p,f} \Big|_{s \rightarrow -\infty} &= \left(\frac{\alpha_s}{\pi}\right)^2 C_F T_F \left[-\frac{1}{48} l_s^4 + \left(1 - \frac{\pi^2}{12}\right) l_s^2 - 3\zeta_3 l_s + \frac{\pi^2}{3} - \frac{\pi^4}{45} \right] \\
&+ \left(\frac{\alpha_s}{\pi}\right)^3 C_F T_F \frac{m^2}{-s} \left[C_F \left(0.0041667l_s^6 - 0.0062500l_s^5 + 0.16629l_s^4 + 1.5817l_s^3 + 1.9782l_s^2 \right. \right. \\
&+ 31.884l_s + 61.904 \left. \right) + C_A \left(0.0010417l_s^6 - 0.022917l_s^5 - 0.12408l_s^4 - 0.14710l_s^3 \right. \\
&- 6.3791l_s^2 - 25.947l_s - 33.440 \left. \right) + T_F n_h \left(0.0083333l_s^5 + 0.023148l_s^4 + 0.14332l_s^3 \right. \\
&+ 2.2434l_s^2 + 4.0771l_s + 3.8620 \left. \right) + T_F n_l \left(0.0083333l_s^5 + 0.023148l_s^4 + 0.14332l_s^3 \right. \\
&\left. + 2.2434l_s^2 + 2.3898l_s - 0.20928 \right) \left. \right], \tag{62}
\end{aligned}$$

where terms of order m^4/s^2 have been dropped. As expected, the scalar and pseudoscalar form factors start at order m^2/s where both develop leading l_s^6 terms. The vector and axial-vector form factors show a similar behavior as in the massless case discussed around Eq. (43).

At threshold the three-loop axial-vector, scalar, and pseudoscalar form factors develop $1/\beta$ poles which are given by

$$F_{1,\text{sing},h}^{a,f} \Big|_{s \rightarrow 4m^2} = \left(\frac{\alpha_s}{\pi}\right)^3 C_F^2 T_F \frac{1}{\beta} [0.062172i l_{2\beta} + 0.097660 - 0.062172i] , \quad (63)$$

$$F_{2,\text{sing},h}^{a,f} \Big|_{s \rightarrow 4m^2} = \left(\frac{\alpha_s}{\pi}\right)^3 C_F^2 T_F \frac{1}{\beta} [-(3.6207 - 1.9240i) l_{2\beta} + 3.0223 + 5.7495i] , \quad (64)$$

$$F_{\text{sing},h}^{s,f} \Big|_{s \rightarrow 4m^2} = \left(\frac{\alpha_s}{\pi}\right)^3 C_F^2 T_F \frac{1}{\beta} [-(2.4674 - 0.8781i) l_{2\beta} + 3.8466 + 2.9977i] , \quad (65)$$

$$F_{\text{sing},h}^{p,f} \Big|_{s \rightarrow 4m^2} = \left(\frac{\alpha_s}{\pi}\right)^3 C_F^2 T_F \frac{1}{\beta} [-(6.0881 - 3.6463i) l_{2\beta} + 5.7276 + 9.5631i] . \quad (66)$$

In Figs. 6 and 7 we show the finite parts of the massive singlet form factors as a function of s .

D One- and two-loop result for $F_{G\tilde{G}}^f$

Our one- and two-loop results for $F_{G\tilde{G}}^f$ are given by

$$F_{G\tilde{G}}^{f,(1)} = -3C_F L_m + C_F \left(-7 + \frac{2\pi^2(1-x)}{3(1+x)} + \frac{(1-x)H_0^2}{2(1+x)} + \frac{2(1-x)H_{0,1}}{1+x} \right) , \quad (67)$$

$$\begin{aligned} F_{G\tilde{G}}^{f,(2)} = & L_m^2 \left\{ -\frac{11}{4} C_F C_A + C_F n_l T_F + C_F^2 \left(\frac{3}{2} + \frac{3(1+x^2)H_0}{2(1-x)(1+x)} \right) \right\} \\ & + L_m \left\{ C_F T_F n_h \left(\frac{8}{3} - \frac{2\pi^2(1-x)}{9(1+x)} - \frac{(1-x)H_0^2}{6(1+x)} - \frac{2(1-x)H_{0,1}}{3(1+x)} \right) \right. \\ & + C_F T_F n_l \left(5 - \frac{4\pi^2(1-x)}{9(1+x)} - \frac{(1-x)H_0^2}{3(1+x)} - \frac{4(1-x)H_{0,1}}{3(1+x)} \right) + C_F C_A \left(-\frac{75}{4} \right. \\ & + \frac{11\pi^2(1-x)}{9(1+x)} + \frac{11(1-x)H_0^2}{12(1+x)} + \frac{11(1-x)H_{0,1}}{3(1+x)} \left. \right) + C_F^2 \left(\frac{29}{4} - \pi^2 \left[\frac{7-8x+7x^2}{12(1-x)(1+x)} \right. \right. \\ & + \left. \left. \frac{(1+x^2)H_0}{3(1+x)^2} \right] + \left[\frac{7(1+x^2)}{2(1-x)(1+x)} - \frac{(1+x^2)H_{0,1}}{(1+x)^2} \right] H_0 - \frac{3(1+x^2)H_{-1}H_0}{(1-x)(1+x)} \right. \\ & \left. + \frac{(1+x+x^2)H_0^2}{2(1-x)(1+x)} - \frac{(1+x^2)H_0^3}{4(1+x)^2} - \frac{(1-x)H_{0,1}}{1+x} + \frac{3(1+x^2)H_{0,-1}}{(1-x)(1+x)} \right) \left. \right\} \\ & + C_F T_F n_h \left(\frac{385}{36} - \pi^2 \left[\frac{3-8x+3x^2}{3(1-x)^2} + \frac{2(1-4x-4x^3+x^4)H_0}{9(1-x)^3(1+x)} \right] \right. \\ & \left. - \frac{(19+8x+19x^2)H_0^2}{18(1-x)^2} - \frac{2(1-4x-4x^3+x^4)H_0^3}{9(1-x)^3(1+x)} \right) + C_F T_F n_l \left(\frac{293}{36} \right. \\ & \left. - \pi^2 \left[\frac{4(5-14x)}{27(1+x)} + \frac{2(1-x)H_0}{9(1+x)} + \frac{8(1-x)H_1}{9(1+x)} \right] - \left[\frac{19(1-x)}{18(1+x)} + \frac{2(1-x)H_1}{3(1+x)} \right] H_0^2 \right) \end{aligned}$$

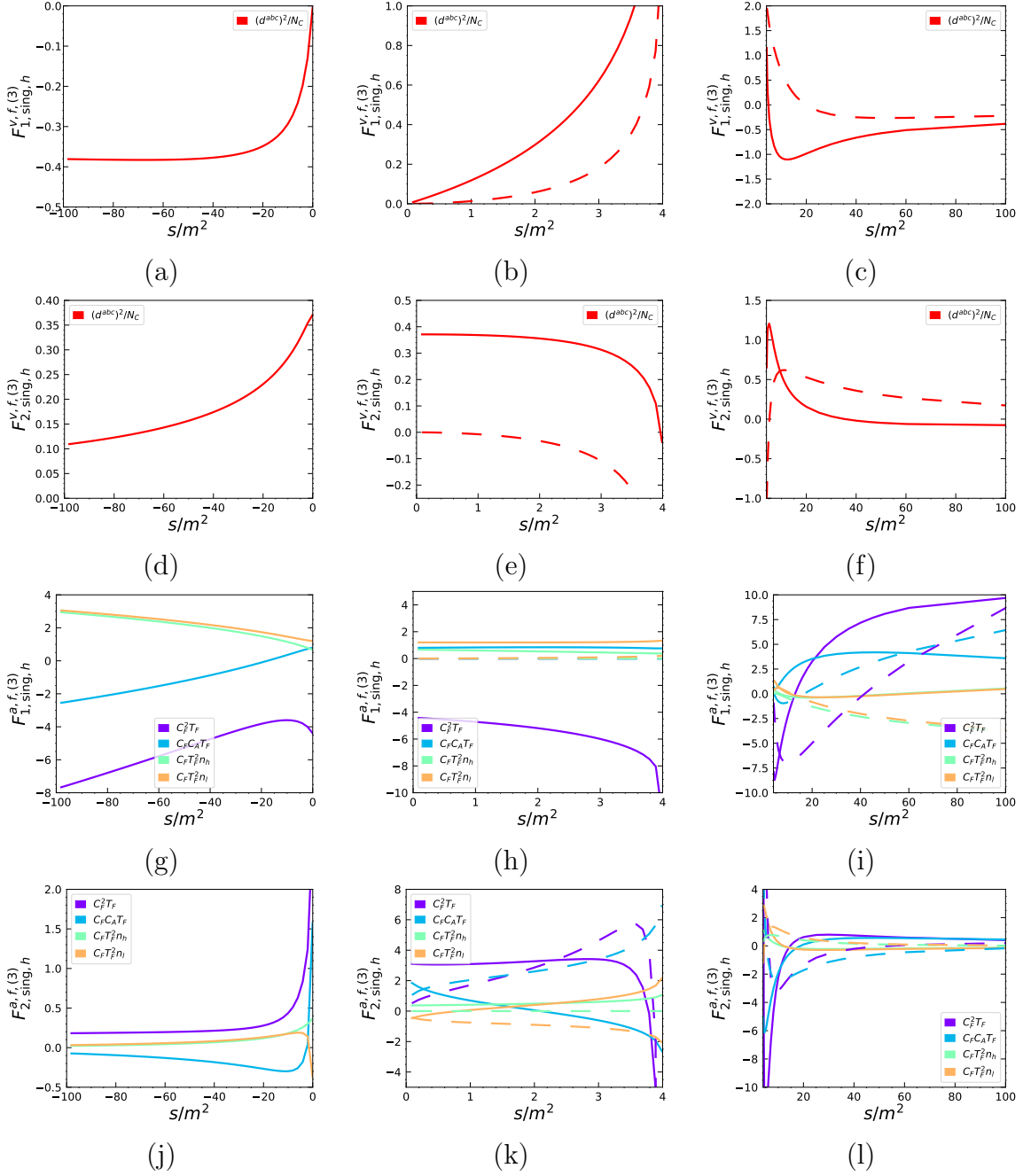


Figure 6: Massive singlet vector and axial-vector form factors as a function of s for $\mu^2 = m^2$.

$$\begin{aligned}
& -\frac{2(1-x)H_0^3}{9(1+x)} - \frac{38(1-x)H_{0,1}}{9(1+x)} - \frac{8(1-x)H_1H_{0,1}}{3(1+x)} - \frac{4(1-x)H_{0,0,1}}{3(1+x)} \\
& + \frac{8(1-x)H_{0,1,1}}{3(1+x)} - \frac{4(1-x)\zeta_3}{3(1+x)} \Big) + C_F C_A \left(-\frac{4963}{144} + \zeta_3 \left[\frac{49 - 75x + 21x^2 + 17x^3}{6(1-x)^2(1+x)} \right. \right.
\end{aligned}$$

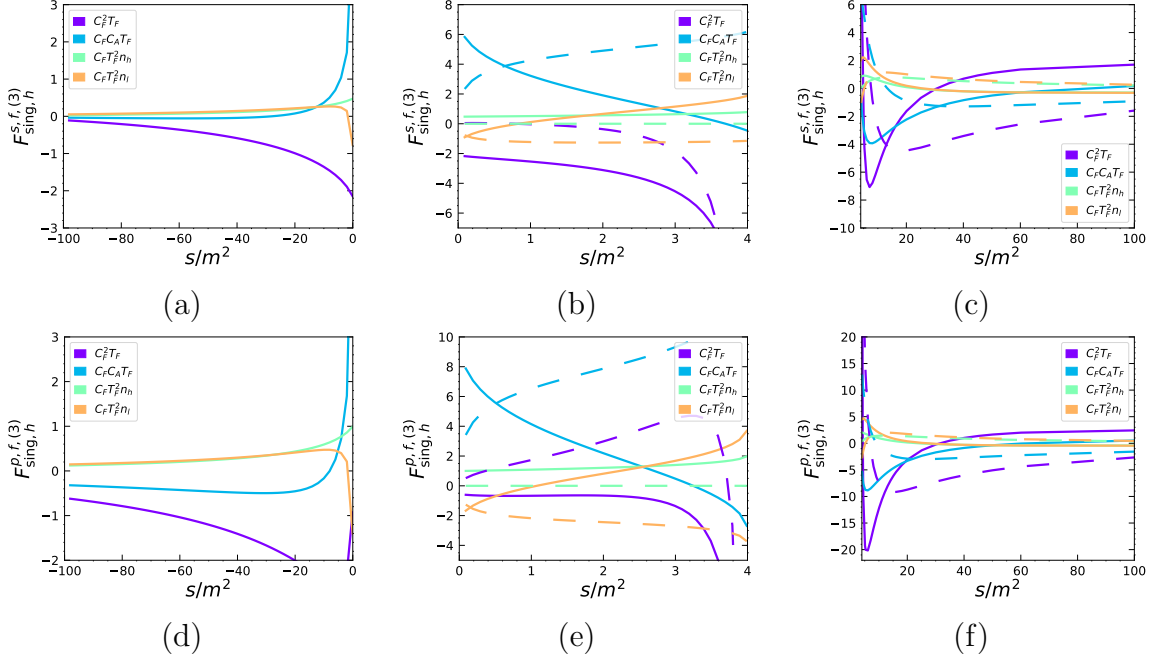


Figure 7: Massive singlet scalar and pseudoscalar form factors as a function of s for $\mu^2 = m^2$.

$$\begin{aligned}
& + \frac{(1 - 4x + 8x^2 - 4x^3 + x^4)H_0}{(1-x)^3(1+x)} \Big] - \frac{\pi^4(29 - 212x + 24x^2 - 212x^3 + 29x^4)}{360(1-x)^3(1+x)} \\
& + \pi^2 \left[\frac{601 - 1803x + 993x^2 - 547x^3}{108(1-x)^2(1+x)} - \left(\frac{-10 + 13x - 12x^2 + 7x^3 + 11x^4}{9(1-x)^3(1+x)} \right. \right. \\
& + \left. \left. \frac{2(1-x)H_1}{3(1+x)} \right) H_0 + \frac{(1 + 2x + 18x^2 + 2x^3 + x^4)H_0^2}{12(1-x)^3(1+x)} - \frac{(5 - 8x + 5x^2)H_{-1}}{2(1-x)^2} \right. \\
& - \frac{(-29 + 159x - 69x^2 + 47x^3)H_1}{18(1-x)^2(1+x)} - \frac{2x(1+x+x^2)H_{0,1}}{(1-x)^3(1+x)} \\
& - \left. \frac{(1 - 4x + 8x^2 - 4x^3 + x^4)H_{0,-1}}{(1-x)^3(1+x)} \right] + \left[\frac{3}{2(1-x)} - \frac{(5+x-5x^2+7x^3)H_{0,1}}{2(1-x)^2(1+x)} \right. \\
& + \frac{(5-8x+5x^2)H_{0,-1}}{(1-x)^2} - \frac{4(1-4x+8x^2-4x^3+x^4)H_{0,0,1}}{(1-x)^3(1+x)} \\
& + \left. \frac{4(1-4x+8x^2-4x^3+x^4)H_{0,0,-1}}{(1-x)^3(1+x)} \right] H_0 + \left[-\frac{-305 + 681x - 717x^2 + 269x^3}{72(1-x)^2(1+x)} \right. \\
& - \frac{(-37 + 63x - 51x^2 + x^3)H_1}{12(1-x)^2(1+x)} + \frac{2(1-4x+7x^2-4x^3+x^4)H_{0,1}}{(1-x)^3(1+x)} \\
& - \left. \frac{(1-4x+8x^2-4x^3+x^4)H_{0,-1}}{(1-x)^3(1+x)} \right] H_0^2 - \frac{(5-8x+5x^2)H_{-1}H_0^2}{2(1-x)^2}
\end{aligned}$$

$$\begin{aligned}
& - \left[\frac{-22 + 46x - 39x^2 + 22x^3 + 29x^4}{36(1-x)^3(1+x)} + \frac{2(1-x)H_1}{3(1+x)} \right] H_0^3 - \frac{(5-8x+5x^2)H_{0,0,-1}}{(1-x)^2} \\
& - \frac{(1-10x-8x^2-10x^3+x^4)H_0^4}{48(1-x)^3(1+x)} + \left[\frac{3}{2} + \frac{19(1-x)H_{0,1}}{3(1+x)} \right] H_1 \\
& + \frac{(287-412x+287x^2)H_{0,1}}{18(1-x)(1+x)} + \frac{(37-3x+93x^2+5x^3)H_{0,0,1}}{6(1-x)^2(1+x)} - \frac{16(1-x)H_{0,1,1}}{3(1+x)} \\
& + \frac{(5-14x+48x^2-14x^3+5x^4)H_{0,0,0,1}}{(1-x)^3(1+x)} - \frac{6(1-4x+8x^2-4x^3+x^4)H_{0,0,0,-1}}{(1-x)^3(1+x)} \\
& + C_F^2 \left(\frac{125}{16} - \frac{\pi^4(-4+12x-16x^2+124x^3-93x^4+31x^5)}{90(1-x)^3(1+x)^2} \right) \\
& - \zeta_3 \left[\frac{3-3x+3x^2+x^3}{(1-x)^2(1+x)} + \frac{2(1-4x+8x^2-4x^3+x^4)H_0}{(1-x)^3(1+x)} \right] \\
& + \pi^2 \left[-\frac{25-42x+x^2+6x^3}{6(1-x)^2(1+x)} + \frac{(-7+12x+22x^2-44x^3+27x^4)H_0}{6(1-x)^3(1+x)} \right. \\
& \left. - \frac{(7-21x+28x^2+68x^3-51x^4+17x^5)H_0^2}{24(1-x)^3(1+x)^2} - \frac{2(1-x)H_1}{3(1+x)} \right. \\
& \left. + \left(\frac{5-8x+5x^2}{(1-x)^2} + \frac{2(1+x^2)H_0}{3(1+x)^2} \right) H_{-1} - \frac{(1+x^2)H_{0,1}}{2(1+x)^2} \right. \\
& \left. + \frac{4(1-3x+4x^2+8x^3-6x^4+2x^5)H_{0,-1}}{3(1-x)^3(1+x)^2} \right] + \left[\frac{3(1+x)}{2(-1+x)} + \frac{4(3-5x+3x^2)H_{0,1}}{(1-x)^2} \right. \\
& \left. - \frac{2(5-8x+5x^2)H_{0,-1}}{(1-x)^2} + \frac{8(1-4x+8x^2-4x^3+x^4)H_{0,0,1}}{(1-x)^3(1+x)} \right. \\
& \left. - \frac{8(1-4x+8x^2-4x^3+x^4)H_{0,0,-1}}{(1-x)^3(1+x)} \right] H_0 + \left[-\frac{1-3x+5x^2+17x^3}{8(1-x)^2(1+x)} \right. \\
& \left. - \frac{(13-11x-5x^2+11x^3)H_1}{2(1-x)^2(1+x)} - \frac{(3-9x+12x^2+4x^3-3x^4+x^5)H_{0,1}}{(1-x)^3(1+x)^2} \right. \\
& \left. + \frac{(3-9x+12x^2+20x^3-15x^4+5x^5)H_{0,-1}}{2(1-x)^3(1+x)^2} \right] H_0^2 \\
& + \frac{(-3+6x+44x^2-70x^3+43x^4)H_0^3}{12(1-x)^3(1+x)} - \frac{3(1-x)H_{0,1}}{1+x} - \frac{2(1-x)H_1H_{0,1}}{1+x} \\
& - \frac{(5-15x+20x^2+44x^3-33x^4+11x^5)H_0^4}{48(1-x)^3(1+x)^2} + \frac{2(1-x)H_{0,1,1}}{1+x} \\
& + \left[\left(-\frac{7(1+x^2)}{(1-x)(1+x)} + \frac{2(1+x^2)H_{0,1}}{(1+x)^2} \right) H_0 + \frac{(5-8x+5x^2)H_0^2}{(1-x)^2} \right. \\
& \left. + \frac{(1+x^2)H_0^3}{2(1+x)^2} \right] H_{-1} - \frac{(1+x^2)H_{0,1}^2}{(1+x)^2} + \left[\frac{7(1+x^2)}{(1-x)(1+x)} - \frac{2(1+x^2)H_{0,1}}{(1+x)^2} \right] H_{0,-1}
\end{aligned}$$

$$\begin{aligned}
& - \frac{2(7 - 6x - 3x^2 + 6x^3)H_{0,0,1}}{(1-x)^2(1+x)} + \frac{2(5 - 8x + 5x^2)H_{0,0,-1}}{(1-x)^2} \\
& - \frac{12(1 - 4x + 8x^2 - 4x^3 + x^4)H_{0,0,0,1}}{(1-x)^3(1+x)} + \frac{12(1 - 4x + 8x^2 - 4x^3 + x^4)H_{0,0,0,-1}}{(1-x)^3(1+x)} \Big), \tag{68}
\end{aligned}$$

with $L_m = \ln(\mu^2/m^2)$ and we dropped the arguments of the harmonic polylogarithms $H_{\vec{w}} \equiv H_{\vec{w}}(x)$ [64].

The one-loop result agrees with Ref. [5], the two-loop expression is new.

E The Fortran library FF31

In this appendix we present the Fortran library **FF31** for the numerical evaluation of the third-order corrections to the form factors. We implement the ultraviolet renormalized form factors, but we do not perform the infrared subtraction. In this way, any infrared subtraction scheme can be applied and it is the task of the user to implement it. The code is available at

<https://gitlab.com/formfactors31/ff31>

where a documentation and sample programs can be found. The code provides interpolation grids and series expansion which can be used for instance in a Monte Carlo program. For the non-singlet contributions interpolation grids are used in the ranges

- $-40 < s/m^2 < 3.75$,
- $4.25 < s/m^2 < 16$,
- $16 < s/m^2 < 60$.

In the remaining regions we implemented the series expansion around $s = \pm\infty$ and $s = 4m^2$. We do not implement the expansion around $s = 16m^2$ since at this point the form factors are continuous functions (but not holomorphic). For the massive singlet contributions interpolation grids are used for

- $-40 < s/m^2 < -1$,
- $1 < s/m^2 < 3.75$,
- $4.25 < s/m^2 < 16$,
- $16 < s/m^2 < 60$,

and for the massless singlet contributions interpolation grids are used in the ranges

- $-40 < s/m^2 < -0.125$,
- $0.125 < s/m^2 < 3.75$,
- $4.25 < s/m^2 < 16$,
- $16 < s/m^2 < 60$.

In the remaining regions we implemented the series expansion around $s = \pm\infty$, $s = 0$, and $s = 4m^2$.

A copy of FF31 can be obtained with

```
$ git clone https://gitlab.com/formfactors31/ff31.git
```

A Fortran compiler such as `gfortran` is needed. The library can be compiled by running

```
$ ./configure  
make
```

The command `make` will generate the static library `libff31.a` which can be linked to the user's program. The module files are located in the directory `modules` which must be also passed to the compiler. This gives access to the public functions and subroutines. The names of all subroutines start with the suffix `ff31_`.

It is instructive to look at a program that uses FF31. We evaluate the vector form factor $F_1^{v,(3)}(s)$ at $s/m^2 = 10$ at order $\epsilon = -3, \dots, 0$ in the ϵ expansion. The fortran program looks as follows:

```
program example1  
  use ff31  
  implicit none  
  
  double complex :: f1v  
  double precision :: s = 10  
  integer :: eporder  
  
  do eporder = -3,0  
    f1v = ff31_veF1(s,eporder)  
    print *, "F1( s = ",s," , ep = ",eporder," ) = ", f1v  
  enddo  
end program example1
```

In the preamble of the program, use `ff3l` loads the respective module. The function `ff3l_veF1` returns the sum of non-singlet, massive, and massless singlet contributions to the ultraviolet renormalized vector form factor F_1^v at three loops and receives two input parameters:

```
double precision :: s
integer :: eporder
```

The variable `s` = s/m^2 is the squared momentum transferred normalized w.r.t. the quark mass. The order in the ϵ is set by the integer `eporder`. Only the values `eporder` = $-3, -2, -1, 0$ are valid. The returned values is a `double complex`, corresponding to the form factor value at third order as an expansion in $\alpha_s^{(n_l+n_h)}(m)$. We assume that the strong coupling constant is renormalized in the $\overline{\text{MS}}$ scheme with the renormalization scale $\mu = m$. The choice whether to use interpolation grids or series expansion is handled internally.

The other types of form factors can be evaluated in a similar way with the functions `ff3l_type` where `type` can be `veF1`, `veF2`, `axF1`, `axF2`, `scF1`, `psF1`. These six routines are implemented for the QCD group SU(3). We implemented also the abelian form factors. The corresponding functions come with the suffix `_qed`, e.g. `ff3l_veF1_qed(s, eporder)`.

By default, if not set explicitly, the library assumes the number of massive and massless quarks to be $n_l = 4$ and $n_h = 1$, respectively. However the user can chose other values, for instance $n_l = 3$ and $n_h = 1$, in the following way:

```
call ff3l_set_nl(3)
call ff3l_set_nh(1)
```

Also by default all contributions from non-singlet and singlet diagrams are included. They can be turned off with

```
call ff3l_nonsinglet_off()
call ff3l_nhsinglet_off()
call ff3l_nlsinglet_off()
```

and turned on with

```
call ff3l_nonsinglet_on()
call ff3l_nhsinglet_on()
call ff3l_nlsinglet_on()
```

In that case the output is the sum of the non-singlet and massive and massless singlet contributions. In case a different linear combination is needed (see, e.g., Eq. (10)), the

individual contributions have to be computed individually using `FF31` and the combination has to be done afterwards.

It is useful to interface the library to Mathematica for simple and fast numerical evaluation and cross checks. To this end, we provide also a Mathematica interface by making use of Wolfram's MathLink interface (for details on the set up see Ref. [72]). The interface is compiled with

```
$ make mathlink
```

To use the library within Mathematica, the interface must be loaded

```
In[] := Install["PATH/ff31"]
```

where `PATH` is the directory where the mathlink executable `ff31` is saved. Form factors in QCD are evaluated with one of the following: `FF31veF1`, `FF31veF2`, `FF31axF1`, `FF31axF2`, `FF31scF1`, `FF31psF1`. For example, the ϵ^0 term of the vector form factor F_1 at third order in α_s is evaluated in the following way:

```
In[] := s = 10;
In[] := eporder = 0;
In[] := FF31veF1[s,eporder]
Out[] := 60.1219 - 172.027 I
```

The number of massless and massive quarks can be set with `FF31SetNl` and `FF31SetNh`. The contribution from non-singlet, n_l - and n_h -singlet diagrams can be switched on and off with the following commands:

```
In[] := FF31NonSingletOff[]
In[] := FF31NonSingletOn[]
In[] := FF31NhSingletOff[]
In[] := FF31NhSingletOn[]
In[] := FF31NlSingletOff[]
In[] := FF31NlSingletOn[]
```

The standalone Mathematica package `formfactors31`, which evaluates the bare and finite form factors, can be found in Ref. [67].

References

- [1] P. Mastrolia and E. Remiddi, Nucl. Phys. B **664** (2003), 341-356 [arXiv:hep-ph/0302162].

- [2] R. Bonciani, P. Mastrolia and E. Remiddi, Nucl. Phys. B **676** (2004), 399-452 [arXiv:hep-ph/0307295].
- [3] W. Bernreuther, R. Bonciani, T. Gehrmann, R. Heinesch, T. Leineweber, P. Mastrolia and E. Remiddi, Nucl. Phys. B **706** (2005), 245-324 [arXiv:hep-ph/0406046].
- [4] W. Bernreuther, R. Bonciani, T. Gehrmann, R. Heinesch, T. Leineweber, P. Mastrolia and E. Remiddi, Nucl. Phys. B **712** (2005), 229-286 [arXiv:hep-ph/0412259].
- [5] W. Bernreuther, R. Bonciani, T. Gehrmann, R. Heinesch, T. Leineweber and E. Remiddi, Nucl. Phys. B **723** (2005), 91-116 [arXiv:hep-ph/0504190].
- [6] W. Bernreuther, R. Bonciani, T. Gehrmann, R. Heinesch, P. Mastrolia and E. Remiddi, Phys. Rev. D **72** (2005), 096002 [arXiv:hep-ph/0508254].
- [7] J. Gluza, A. Mitov, S. Moch and T. Riemann, JHEP **07** (2009), 001 [arXiv:0905.1137 [hep-ph]].
- [8] J. Henn, A. V. Smirnov, V. A. Smirnov and M. Steinhauser, JHEP **01** (2017), 074 [arXiv:1611.07535 [hep-ph]].
- [9] T. Ahmed, J. M. Henn and M. Steinhauser, JHEP **06** (2017), 125 [arXiv:1704.07846 [hep-ph]].
- [10] J. Ablinger, A. Behring, J. Blümlein, G. Falcioni, A. De Freitas, P. Marquard, N. Rana and C. Schneider, Phys. Rev. D **97** (2018), 094022 [arXiv:1712.09889 [hep-ph]].
- [11] R. N. Lee, A. V. Smirnov, V. A. Smirnov and M. Steinhauser, JHEP **03** (2018), 136 [arXiv:1801.08151 [hep-ph]].
- [12] M. Fael, F. Lange, K. Schönwald and M. Steinhauser, Phys. Rev. Lett. **128** (2022), 172003 [arXiv:2202.05276 [hep-ph]].
- [13] M. Fael, F. Lange, K. Schönwald and M. Steinhauser, Phys. Rev. D **106** (2022), 034029 [arXiv:2207.00027 [hep-ph]].
- [14] R. N. Lee, A. V. Smirnov, V. A. Smirnov and M. Steinhauser, JHEP **05** (2018), 187 [arXiv:1804.07310 [hep-ph]].
- [15] J. Ablinger, J. Blümlein, P. Marquard, N. Rana and C. Schneider, Phys. Lett. B **782** (2018), 528-532 [arXiv:1804.07313 [hep-ph]].
- [16] J. Ablinger, J. Blümlein, P. Marquard, N. Rana and C. Schneider, Nucl. Phys. B **939** (2019), 253-291 [arXiv:1810.12261 [hep-ph]].
- [17] J. Blümlein, P. Marquard, N. Rana and C. Schneider, Nucl. Phys. B **949** (2019), 114751 [arXiv:1908.00357 [hep-ph]].

- [18] X. Chen, X. Guan, C.-Q. He, X. Liu and Y.-Q. Ma, [arXiv:2209.14259 [hep-ph]].
- [19] R. N. Lee, A. von Manteuffel, R. M. Schabinger, A. V. Smirnov, V. A. Smirnov and M. Steinhauser, Phys. Rev. Lett. **128** (2022), 212002 [arXiv:2202.04660 [hep-ph]].
- [20] P. A. Baikov, K. G. Chetyrkin, A. V. Smirnov, V. A. Smirnov and M. Steinhauser, Phys. Rev. Lett. **102** (2009), 212002 [arXiv:0902.3519 [hep-ph]].
- [21] R. N. Lee, A. V. Smirnov and V. A. Smirnov, JHEP **04** (2010), 020 [arXiv:1001.2887 [hep-ph]].
- [22] T. Gehrmann, E. W. N. Glover, T. Huber, N. Ikizlerli and C. Studerus, JHEP **06** (2010), 094 [arXiv:1004.3653 [hep-ph]].
- [23] L. Chen, M. Czakon and M. Niggetiedt, JHEP **12** (2021), 095 [arXiv:2109.01917 [hep-ph]].
- [24] S. A. Larin and J. A. M. Vermaseren, Phys. Lett. B **259** (1991), 345-352.
- [25] S. A. Larin, Phys. Lett. B **303** (1993), 113-118 [arXiv:hep-ph/9302240].
- [26] S. L. Adler, Phys. Rev. **177** (1969), 2426-2438.
- [27] J. S. Bell and R. Jackiw, Nuovo Cim. A **60** (1969), 47-61.
- [28] A. M. Polyakov, Nucl. Phys. B **164** (1980), 171-188.
- [29] G. P. Korchemsky and A. V. Radyushkin, Nucl. Phys. B **283** (1987), 342-364.
- [30] A. Grozin, J. M. Henn, G. P. Korchemsky and P. Marquard, Phys. Rev. Lett. **114** (2015), 062006 [arXiv:1409.0023 [hep-ph]].
- [31] A. G. Grozin, J. M. Henn, G. P. Korchemsky and P. Marquard, JHEP **01** (2016), 140 [arXiv:1510.07803 [hep-ph]].
- [32] S. L. Adler and W. A. Bardeen, Phys. Rev. **182** (1969), 1517-1536.
- [33] M. F. Zoller, JHEP **07** (2013), 040 [arXiv:1304.2232 [hep-ph]].
- [34] T. Ahmed, T. Gehrmann, P. Mathews, N. Rana and V. Ravindran, JHEP **11** (2015), 169 [arXiv:1510.01715 [hep-ph]].
- [35] T. Ahmed, L. Chen and M. Czakon, JHEP **05** (2021), 087 [arXiv:2101.09479 [hep-ph]].
- [36] M. Lüscher and P. Weisz, Eur. Phys. J. C **81** (2021), 519 [arXiv:2103.15440 [hep-ph]].
- [37] L. Chen and M. Czakon, JHEP **01** (2022), 187 [arXiv:2112.03795 [hep-ph]].

- [38] P. Nogueira, J. Comput. Phys. **105** (1993), 279-289;
<http://cfif.ist.utl.pt/~paulo/qgraf.html>.
- [39] R. Harlander, T. Seidensticker and M. Steinhauser, Phys. Lett. B **426** (1998), 125-132 [arXiv:hep-ph/9712228].
- [40] T. Seidensticker, arXiv:hep-ph/9905298.
- [41] <http://sfb-tr9.ttp.kit.edu/software/html/q2eexp.html>.
- [42] J. Kuipers, T. Ueda, J. A. M. Vermaseren and J. Vollinga, Comput. Phys. Commun. **184** (2013), 1453-1467 [arXiv:1203.6543 [cs.SC]].
- [43] P. Maierhöfer, J. Usovitsch and P. Uwer, Comput. Phys. Commun. **230** (2018), 99-112 [arXiv:1705.05610 [hep-ph]].
- [44] J. Klappert, F. Lange, P. Maierhöfer and J. Usovitsch, Comput. Phys. Commun. **266** (2021), 108024 [arXiv:2008.06494 [hep-ph]].
- [45] R. H. Lewis, Fermat User's Guide, <http://home.bway.net/lewis>.
- [46] A. V. Smirnov and V. A. Smirnov, Nucl. Phys. B **960** (2020), 115213 [arXiv:2002.08042 [hep-ph]].
- [47] R. N. Lee, arXiv:1212.2685 [hep-ph].
- [48] R. N. Lee, J. Phys. Conf. Ser. **523** (2014), 012059 [arXiv:1310.1145 [hep-ph]].
- [49] M. Fael, F. Lange, K. Schönwald and M. Steinhauser, JHEP **09** (2021), 152 [arXiv:2106.05296 [hep-ph]].
- [50] M. Gerlach, F. Herren and M. Lang, Comput. Phys. Commun. **282** (2023), 108544 [arXiv:2201.05618 [hep-ph]].
- [51] X. Liu and Y.-Q. Ma, Comput. Phys. Commun. **283** (2023), 108565 [arXiv:2201.11669 [hep-ph]].
- [52] X. Liu, Y.-Q. Ma and C.-Y. Wang, Phys. Lett. B **779** (2018), 353-357 [arXiv:1711.09572 [hep-ph]].
- [53] X. Liu, Y.-Q. Ma, W. Tao and P. Zhang, Chin. Phys. C **45** (2021), 013115 [arXiv:2009.07987 [hep-ph]].
- [54] X. Liu and Y.-Q. Ma, Phys. Rev. D **105** (2022), L051503 [arXiv:2107.01864 [hep-ph]].
- [55] Z.-F. Liu and Y.-Q. Ma, Phys. Rev. D **105** (2022), 074003 [arXiv:2201.11636 [hep-ph]].

- [56] Z.-F. Liu and Y.-Q. Ma, Phys. Rev. Lett. **129** (2022), 222001 [arXiv:2201.11637 [hep-ph]].
- [57] S. Gerhold, Diploma Thesis, J. Kepler University, Linz, 2002.
- [58] C. Schneider, Sém. Lothar. Combin. **56** (2007), B56b; C. Schneider, in: Computer Algebra in Quantum Field Theory: Integration, Summation and Special Functions Texts and Monographs in Symbolic Computation eds. C. Schneider and J. Blümlein (Springer, Wien, 2013), 325–360 [arXiv:1304.4134 [cs.SC]].
- [59] J. A. M. Vermaseren, Int. J. Mod. Phys. A **14** (1999), 2037-2076 [arXiv:hep-ph/9806280]; J. Blümlein, Comput. Phys. Commun. **180** (2009), 2218-2249 [arXiv:0901.3106 [hep-ph]]; J. Ablinger, Diploma Thesis, J. Kepler University Linz, 2009, arXiv:1011.1176 [math-ph]; J. Ablinger, J. Blümlein and C. Schneider, J. Math. Phys. **52** (2011), 102301 [arXiv:1105.6063 [math-ph]]; J. Ablinger, J. Blümlein and C. Schneider, J. Math. Phys. **54** (2013), 082301 [arXiv:1302.0378 [math-ph]]; J. Ablinger, Ph.D. Thesis, J. Kepler University Linz, 2012, arXiv:1305.0687 [math-ph]; J. Ablinger, J. Blümlein and C. Schneider, J. Phys. Conf. Ser. **523** (2014), 012060 [arXiv:1310.5645 [math-ph]]; J. Ablinger, J. Blümlein, C. G. Raab and C. Schneider, J. Math. Phys. **55** (2014), 112301 [arXiv:1407.1822 [hep-th]]; J. Ablinger, PoS **LL2014** (2014), 019 [arXiv:1407.6180 [cs.SC]]; J. Ablinger, arXiv:1606.02845 [cs.SC]; J. Ablinger, PoS **RADCOR2017** (2017), 001 [arXiv:1801.01039 [cs.SC]]; J. Ablinger, PoS **LL2018** (2018), 063; J. Ablinger, arXiv:1902.11001 [math.CO].
- [60] M. Beneke and V. A. Smirnov, Nucl. Phys. B **522** (1998), 321-344 [arXiv:hep-ph/9711391].
- [61] B. Jantzen, A. V. Smirnov and V. A. Smirnov, Eur. Phys. J. C **72** (2012), 2139 [arXiv:1206.0546 [hep-ph]].
- [62] J. Fleischer, M. Y. Kalmykov and A. V. Kotikov, Phys. Lett. B **462** (1999), 169-177 [erratum: Phys. Lett. B **467** (1999), 310-310] [arXiv:hep-ph/9905249].
- [63] E. Panzer, Comput. Phys. Commun. **188** (2015), 148-166 [arXiv:1403.3385 [hep-th]].
- [64] E. Remiddi and J. A. M. Vermaseren, Int. J. Mod. Phys. A **15** (2000), 725-754 [arXiv:hep-ph/9905237].
- [65] <https://www.ttp.kit.edu/preprints/2023/ttp23-002/>.
- [66] A. V. Smirnov, N. D. Shapurov and L. I. Vysotsky, Comput. Phys. Commun. **277** (2022), 108386 [arXiv:2110.11660 [hep-ph]].
- [67] <https://gitlab.com/formfactors3l/formfactors3l>.
- [68] <https://gitlab.com/formfactors3l/ff3l>.

- [69] H. R. P. Ferguson, D. H. Bailey and S. Arno, *Math. Comp.* **68** (1999), 351-369.
- [70] J. A. M. Vermaseren, *Comput. Phys. Commun.* **83** (1994), 45-58.
- [71] D. Binosi and L. Theußl, *Comput. Phys. Commun.* **161** (2004), 76-86 [arXiv:hep-ph/0309015].
- [72] T. Hahn, *Comput. Phys. Commun.* **183** (2012), 460–469 [arXiv:1107.4379 [physics.comp-ph]].